NASA TECHNICAL NOTE

NASA TN D-5408

NASA TN D-5408

STATIC AND DYNAMIC STABILITY DERIVATIVES OF A MODEL OF A JET TRANSPORT EQUIPPED WITH EXTERNAL-FLOW JET-AUGMENTED FLAPS

by Delma C. Freeman, Jr., Sue B. Grafton, and Richard D'Amato

Langley Research Center
Langley Station, Hampton, Va.

NATIONAL AERONAUTICS AND SPACE ADMINISTRATION • WASHINGTON, D. C. • SEPTEMBER 1969

1. Report No. NASA TN D-5408	2. Government Accession No.	3. Recipient's Catalog No.
4. Title and Subtitle STATIC AND DYNAMIC STABILITY DERIVATIVES OF A MODEL OF A JET TRANSPORT EQUIPPED WITH EXTERNAL-FLOW JET-AUGMENTED FLAPS		5. Report Date September 1969
		6. Performing Organization Code
7. Author(s) Delma C. Freeman, Jr., Sue B. Grafton, and Richard D'Amato		8. Performing Organization Report No. L-6521
9. Performing Organization Name and Address NASA Langley Research Center Hampton, Va. 23365		10. Work Unit No. 721-01-11-03-23
		11. Contract or Grant No.
		13. Type of Report and Period Covered Technical Note
12. Sponsoring Agency Name and Address National Aeronautics and Space Administration Washington, D.C. 20546		14. Sponsoring Agency Code
15. Supplementary Notes		

16. Abstract

A wind-tunnel investigation has been made to determine the static and dynamic stability derivatives of a model of a large jet transport equipped with external-flow jet-augmented flaps. The tests were conducted in the Langley full-scale tunnel, and a model powered by scale-model, compressed-air-driven turbofan engines was used.

The results of the investigation showed that blowing on the flap system increased the lift-curve slope, delayed the stall, and increased the maximum lift coefficient. The data also showed that all model configurations generally had static longitudinal stability over the test angle-of-attack range except those at the higher flap-deflection angles where the effects of power were destabilizing. The results also showed that the model had positive damping in pitch, roll, and yaw throughout the test angle-of-attack range up to and slightly beyond the stall for all test conditions. The application of power in the flap system resulted in appreciable increases in roll damping but produced essentially no effects in pitch and yaw damping. There were essentially no effects due to oscillation frequency on the damping derivatives.

17. Key Words Suggested by Author(s) Jet-augmented flaps Dynamic stability	18. Distribution Statement Unclassified – Unlimited		
19. Security Classif. (of this report) Unclassified	20. Security Classif. (of this page) Unclassified	21. No. of Pages 50	22. Price* $3.00

*For sale by the Clearinghouse for Federal Scientific and Technical Information
Springfield, Virginia 22151

STATIC AND DYNAMIC STABILITY DERIVATIVES OF A MODEL OF A JET TRANSPORT EQUIPPED WITH EXTERNAL-FLOW JET-AUGMENTED FLAPS

By Delma C. Freeman, Jr., Sue B. Grafton,
and Richard D'Amato
Langley Research Center

SUMMARY

A wind-tunnel investigation has been made to determine the static and dynamic stability derivatives of a model of a large jet transport equipped with external-flow jet-augmented flaps. The tests were conducted in the Langley full-scale tunnel, and a model powered by scale-model, compressed-air-driven turbofan engines was used.

The results of the investigation showed that blowing on the flap system increased the lift-curve slope, delayed the stall, and increased the maximum lift coefficient. The data also showed that all model configurations generally had static longitudinal stability over the test angle-of-attack range except those at the higher flap-deflection angles where the effects of power were destabilizing. The results also showed that the model had positive damping in pitch, roll, and yaw throughout the test angle-of-attack range up to and slightly beyond the stall for all test conditions. The application of power in the flap system resulted in appreciable increases in roll damping but produced essentially no effects in pitch and yaw damping. There were essentially no effects due to oscillation frequency on the damping derivatives.

INTRODUCTION

A great deal of interest has been shown in the external-flow jet-augmented-flap concept as a means of achieving high lift coefficients. In this concept, the jet efflux from pod-mounted engines is deflected upward to blow over the flaps and through slots of the flaps and, thus, induces very high lift on the wing. Early experimental investigations of external-flow jet-augmented flaps on general research models (for example, see refs. 1 to 5) have demonstrated that desirably high lift coefficients can be generated with this system. Recently, a program has been started at the Langley Research Center to investigate the application of the external-flow jet-augmented flap to a large jet transport with high bypass-ratio turbofan engines. The results of conventional static wind-tunnel tests of this configuration are reported in reference 6 and show that the external-flow jet-augmented flap offered a promising means of achieving improved take-off and landing

performance for large jet transports. Because of these promising results, a program has been initiated to evaluate the dynamic stability, flight characteristics, and general piloting techniques of such a configuration. This work is to be conducted with a fixed-base simulator requiring aerodynamic inputs in the form of static and dynamic stability derivatives of the particular configuration under study. As part of the overall program, the present investigation was undertaken to measure the static and dynamic stability derivatives of the jet-transport model with an external-flow jet-augmented flap.

The model used in the investigation was powered by four high-bypass-ratio turbofan engines and could be equipped with double-slotted trailing-edge flaps for use in an external-flow jet-augmented-flap system. The flap configurations tested represented possible landing-approach and take-off configurations. The dynamic stability derivatives were determined in pitching, rolling, and yawing forced-oscillation tests at two different frequencies over an angle-of-attack range. In order to help interpret the dynamic data, the static longitudinal and lateral stability characteristics of the model were also determined and are presented.

SYMBOLS

The longitudinal data are referred to the stability-axis system and the lateral data are referred to the body-axis system. (See fig. 1.) The origin of the axes was located to correspond to the center-of-gravity position (0.25 mean aerodynamic chord) shown in figure 2.

In order to facilitate international usage of data presented, dimensional quantities are presented both in the U.S. Customary Units and in the International System of Units (SI). Equivalent dimensions were determined by using the conversion factors given in reference 7.

b	wing span, feet (meters)
C_{L_α}	lift-curve slope, $\frac{\partial C_L}{\partial \alpha}$
c	local wing chord, inches (centimeters)
$\bar{c}$	mean aerodynamic chord, feet (meters)
F_D	drag force, pounds (newtons)
F_L	lift force, pounds (newtons)
F_X	force along X-axis, pounds (newtons)

F_Y	lateral force, pounds (newtons)
F_Z	force along Z-axis, pounds (newtons)
f	frequency of oscillation, cycle/second (1 cycle/second = 1 hertz)
i_t	horizontal-tail incidence angle, degrees
k	reduced-frequency parameter, $\omega b/2V$ or $\omega \bar{c}/2V$
M_X	rolling moment, foot-pounds (meter-newtons)
M_Y	pitching moment, foot-pounds (meter-newtons)
M_Z	yawing moment, foot-pounds (meter-newtons)
p	rolling velocity, radians/second
q	pitching velocity, radians/second
q_∞	free-stream dynamic pressure, $\rho V^2/2$, pounds/foot^2 (newtons/meter^2)
r	yawing velocity, radians/second
S	wing area, feet^2 (meters^2)
T	thrust, pounds (newtons)
V	free-stream velocity, feet/second (meters/second)
X,Y,Z	body reference axes
X_S, Y_S, Z_S	stability reference axes
α	angle of attack, degrees or radians
$\dot{\alpha}$	rate of change of angle of attack, radians/second
β	angle of sideslip, degrees or radians

$\dot{\beta}$ rate of change of angle of sideslip, radians/second

δ_e elevator deflection, positive when trailing edge down, degrees

δ_{f1} forward trailing-edge flap-segment deflection, degrees

δ_{f2} aft trailing-edge flap-segment deflection, degrees

δ_{sl} leading-edge slat deflection, degrees

ρ air density, slugs/foot^3 (kilograms/meter^3)

ϕ angle of roll, degrees or radians

ω angular velocity, $2\pi f$, radians/second

$$C_X = \frac{F_X}{q_\infty S} \qquad C_Z = \frac{F_Z}{q_\infty S} \qquad C_m = \frac{M_Y}{q_\infty S\bar{c}}$$

$$C_{X_q} = \frac{\partial C_X}{\partial \frac{q\bar{c}}{2V}} \qquad C_{Z_q} = \frac{\partial C_Z}{\partial \frac{q\bar{c}}{2V}} \qquad C_{m_q} = \frac{\partial C_m}{\partial \frac{q\bar{c}}{2V}}$$

$$C_{X_{\dot{\alpha}}} = \frac{\partial C_X}{\partial \frac{\dot{\alpha}\bar{c}}{2V}} \qquad C_{Z_{\dot{\alpha}}} = \frac{\partial C_Z}{\partial \frac{\dot{\alpha}\bar{c}}{2V}} \qquad C_{m_{\dot{\alpha}}} = \frac{\partial C_m}{\partial \frac{\dot{\alpha}\bar{c}}{2V}}$$

$$C_D = \frac{F_D}{q_\infty S} \qquad C_L = \frac{F_L}{q_\infty S} \qquad C_T = \frac{T}{q_\infty S}$$

$$C_l = \frac{M_X}{q_\infty Sb} \qquad C_n = \frac{M_Z}{q_\infty Sb} \qquad C_Y = \frac{F_Y}{q_\infty S}$$

$$C_{l_p} = \frac{\partial C_l}{\partial \frac{pb}{2V}} \qquad C_{n_p} = \frac{\partial C_n}{\partial \frac{pb}{2V}} \qquad C_{Y_p} = \frac{\partial C_Y}{\partial \frac{pb}{2V}}$$

$$C_{l_r} = \frac{\partial C_l}{\partial \frac{rb}{2V}} \qquad C_{n_r} = \frac{\partial C_n}{\partial \frac{rb}{2V}} \qquad C_{Y_r} = \frac{\partial C_Y}{\partial \frac{rb}{2V}}$$

$$C_{l_{\dot{\beta}}} = \frac{\partial C_l}{\partial \frac{\dot{\beta}b}{2V}} \qquad C_{n_{\dot{\beta}}} = \frac{\partial C_n}{\partial \frac{\dot{\beta}b}{2V}} \qquad C_{Y_{\dot{\beta}}} = \frac{\partial C_Y}{\partial \frac{\dot{\beta}b}{2V}}$$

$$C_{l_\beta} = \frac{\partial C_l}{\partial \beta} \qquad C_{n_\beta} = \frac{\partial C_n}{\partial \beta} \qquad C_{Y_\beta} = \frac{\partial C_Y}{\partial \beta}$$

TESTS, EQUIPMENT, AND TECHNIQUE

Wind Tunnel

The tests were made in the 30- by 60-foot (9.1- by 18.3-meter) open-throat test section of the Langley full-scale tunnel with the model mounted about 10 feet (3.05 meters) above the ground board. The model was so small in proportion to the tunnel test section that no wind-tunnel wall corrections were needed or applied. Normal corrections for flow angularity were applied.

Apparatus and Model

The investigation was conducted on the four-engine, high-wing, jet-transport model illustrated by the three-view drawing of figure 2(a). The dimensional characteristics of the model are given in table I. The wing had an average leading-edge sweep angle of 28° and incorporated leading-edge slats and double-slotted trailing-edge flaps. A detailed sketch of the flap assembly and engine-pylon arrangement is shown in figure 2(b). The wing airfoil section was the same as that used in reference 6. The forward and aft flap-deflection angles tested represent approximately a landing-approach condition $\left(\delta_{f1}/\delta_{f2} = 30^{\circ}/60^{\circ}\right)$ and take-off conditions $\left(\delta_{f1}/\delta_{f2} = 20^{\circ}/40^{\circ} \text{ and } \delta_{f1}/\delta_{f2} = 10^{\circ}/20^{\circ}\right)$. The slat-deflection angles represent these same conditions. Photographs of the model and flap system are shown in figures 3(a) and 3(b), respectively.

To facilitate model configuration changes and to insure accurate flap-deflection angles, the wing of the model was designed with removable trailing edges. To convert the model from the clean configuration to each of the flap-deflected configurations, the clean trailing edges were replaced with trailing-edge flaps constructed with fixed gaps, overlaps, and deflection angles. The leading-edge slats were designed so that they could be fastened to the wing leading edge at fixed positions when desired.

The model engines represented high-bypass-ratio turbofans and were installed at -3° incidence so that the jet exhaust impinged directly on the trailing-edge flap system. The engine turbines were driven by compressed air and turned fans which produced the desired thrust.

All dynamic force tests were made with a single strut and sting support system and a strain-gage balance. Sketches of the forced-oscillation test equipment are presented in figure 4, and the equipment is described in reference 8. The static force tests were made on a conventional sting which entered the rear of the fuselage.

Tests and Procedures

Calibrations were made to determine the engine-installed thrust as a function of engine speed in revolutions per minute with the model at an angle of attack of 0° and with

the trailing-edge flaps and leading-edge slats undeflected. The aerodynamic tests were made by setting the engine speed to give the desired thrust at an angle of attack of 0° and then maintaining this engine speed as the model was tested through a range of angles of attack.

The thrust calibrations were made at the free-stream dynamic pressure used in the present tests, 7.1 lb/ft^2 $(340\ N/m^2)$. The value for the thrust used in computing the thrust coefficients for the forward flight tests is the difference between the longitudinal force with power on and the longitudinal force with power off and flow-through nacelles, both for the same free-stream dynamic pressure. The longitudinal force with power off and flow-through nacelles was not actually measured on the present model but was computed by subtracting the increment of drag coefficient due to the windmilling of rotating parts from the drag coefficient of the model in the windmilling condition. The drag of the windmilling parts was assumed to be the same as that measured for similar but 60-percent larger scale-model engines in an unpublished investigation. There is the possibility of a small error in this procedure if the drag coefficient of the windmilling parts is not exactly the same on the larger and smaller engines. Even if the assumed drag coefficient of the windmilling parts of the present engines were 100-percent different, however, the error in thrust coefficient would only be about 5 percent for the lowest thrust coefficient of the tests and would be even smaller for the higher thrust coefficients. The thrust calibrations were made through a range of engine speeds up to 60 000 revolutions per minute, at which speed the fans developed, in the static condition, their rated thrusts of approximately 30 pounds (133.44 newtons) each.

Dynamic-force tests were made to determine the longitudinal and lateral oscillatory stability derivatives of all model configurations with power off and for thrust coefficients C_T of 0.38, 0.78, and 1.70. These force tests were made over an angle-of-attack range from -4° to 24° for the three flap-deflection combinations previously discussed. The dynamic stability derivatives were measured for an amplitude of 5.5° and for frequencies of 0.5 and 1.0 cycle per second corresponding to values of the reduced-frequency parameter k of 0.023 and 0.045, respectively, for the pitching tests and 0.160 and 0.321, respectively, for both the rolling and yawing tests. In order to help interpret the dynamic data, static-force tests were also conducted to obtain the static longitudinal and lateral stability characteristics of the model. All tests were conducted with the rudder undeflected and with the tail incidence and elevator-deflection angle set to give longitudinal trim in the operational angle-of-attack range of the airplane.

The force tests were conducted at a dynamic pressure of 7.1 lb/ft^2 $(340\ N/m^2)$ which corresponds to a Reynolds number of 0.543×10^6 based on the mean aerodynamic chord of the model.

RESULTS AND DISCUSSION

Static Stability Derivatives

Longitudinal.- The static longitudinal stability derivatives of the model are presented in figure 5. In general the data show that blowing on the flap system increased the lift-curve slope, delayed the stall, and increased the maximum lift coefficient. A maximum lift coefficient of 4.4 was achieved by using the landing-approach flap system $\left(\delta_{f1}/\delta_{f2} = 30^{o}/60^{o}\right)$ with maximum thrust $\left(C_T = 1.70\right)$. The data show that all the model configurations generally had static longitudinal stability over the test angle-of-attack range for the power-off condition. The effects of power were small at the lower flap-deflection angles, but at the higher deflection angles these effects were destabilizing and actually caused the model to become unstable at negative angles of attack. The horizontal-tail incidence and elevator deflection used in the investigation were approximately correct for providing longitudinal trim.

Lateral.- The static lateral stability derivatives of the model are presented in figures 6 and 7. The data of figure 6 show that the variation of C_l, C_n, and C_Y is generally linear over the range of sideslip angles measured ($\beta = \pm 5^{o}$) at all but the highest angle of attack tested ($\alpha = 25.2^{o}$), which was generally near, or above, the stall. The data presented in figure 7 were determined from the incremental differences in C_l, C_n, and C_Y at angles of sideslip ranging from -5^{o} to 5^{o}. These data show that the clean configuration had directional stability $\left(+C_{n_\beta}\right)$ and positive dihedral effect $\left(-C_{l_\beta}\right)$ for angles of attack up to about 15^{o}. Deflecting the leading-edge slats and trailing-edge flaps increased the level of directional stability for the power-off condition, but application of power generally caused a reduction in directional stability. Generally, except at $\delta_{f1}/\delta_{f2} = 0^{o}/0^{o}$ and $\delta_{f1}/\delta_{f2} = 10^{o}/20^{o}$, the model had positive dihedral effect $\left(-C_{l_\beta}\right)$ throughout the test angle-of-attack range. For the higher flap-deflection angles $\left(\delta_{f1}/\delta_{f2} = 20^{o}/40^{o}\right.$ and $\left.\delta_{f1}/\delta_{f2} = 30^{o}/60^{o}\right)$, the effect of power was to markedly increase the positive dihedral effect.

Dynamic Stability Derivatives

Pitching.- The variation of oscillatory pitching derivatives with angle of attack is presented in figures 8 and 9. The data show that the model had positive damping in pitch $\left(\text{negative values of } C_{m_q} + C_{m_{\dot{\alpha}}}\right)$ throughout the test angle-of-attack range for all test conditions. The data also show that there were essentially no effects of power on the pitch damping for angles of attack below the stall. At the stall changes in the pitch damping occurred, which might be associated with separation effects on the wing or possibly with some alteration of the downwash at the horizontal tail. At the higher angles of attack, the power generally increased the pitch damping for all flap-deflection angles. This increased damping probably can be attributed to the delay in the stall associated with the

application of power. The data of figure 9 show that oscillation frequency had no appreciable effect on the pitch damping in the normal operating angle-of-attack range of this configuration.

Rolling.- The variation of the lateral oscillatory rolling derivatives with angle of attack are presented in figures 10 and 11. These data show that the model had positive damping in roll $\left(\text{negative values of } C_{l_p} + C_{l_{\dot{\beta}}} \sin \alpha\right)$ throughout the test angle-of-attack range for all test conditions. The effect of power was to increase the roll damping. This result was expected since the damping in roll is dependent upon the lift-curve slope, and the data of figure 5 show that substantial increases in lift-curve slope occur with increased power. The relationship between the increase in lift-curve slope and the increase in roll damping due to the power is indicated in figure 12. These data show considerable scatter but indicate that the percent increase in roll damping due to power was only about one-half as great as the percent increase in lift-curve slope. The probable reasons for this result are that the comparison is made for the complete airplane ignoring any effects of the vertical tail and that most of the power-induced lift, and consequently the power-induced increase in lift-curve slope, is produced on the inboard sections of the wing where the moment arm for producing rolling moments is small.

Yawing.- The variation of the lateral oscillatory yawing derivatives with angle of attack is presented in figures 13 and 14. These data show that the model had positive yaw damping $\left(\text{negative values of } C_{n_r} - C_{n_{\dot{\beta}}} \cos \alpha\right)$ throughout the test angle-of-attack range for all test conditions. For angles of attack below the stall, there appeared to be only small effects of power on the yaw damping. The data also show that the roll-due-to-yawing parameter $\left(C_{l_r} - C_{l_{\dot{\beta}}} \cos \alpha\right)$ was positive and increased with increasing angle of attack up to the stall. The data of figure 14 show a slight effect of frequency for the power-off condition.

SUMMARY OF RESULTS

The results of an investigation to determine the static and dynamic stability derivatives of a model of a large jet transport equipped with an external-flow jet-augmented flap may be summarized as follows:

1. The static longitudinal data show that blowing on the flap system increased the lift-curve slope, delayed the stall, and increased the maximum lift coefficient. The data also show that all the model configurations generally had static longitudinal stability over the test angle-of-attack range and that at the higher deflection angles the effects of power were destabilizing.

2. The effects of power generally were to reduce the directional stability and to increase the positive dihedral effect especially for higher flap-deflection angles.

3. The model had positive damping in pitch, roll, and yaw throughout the test angle-of-attack range up to and slightly beyond the stall for all test conditions.

4. The application of power in the jet-augmented-flap system resulted in appreciable increases in roll damping but produced essentially no effects in pitch and yaw damping. The percent increase in the roll damping associated with power was found to be about one-half as great as the percent increase in the lift-curve slope.

5. There were essentially no effects due to oscillation frequency on the damping derivatives.

Langley Research Center,
National Aeronautics and Space Administration,
Langley Station, Hampton, Va., June 5, 1969,
721-01-11-03-23.

REFERENCES

1. Campbell, John P.; and Johnson, Joseph L., Jr.: Wind-Tunnel Investigation of an External-Flow Jet-Augmented Slotted Flap Suitable for Application to Airplanes With Pod-Mounted Jet Engines. NACA TN 3898, 1956.

2. Lowry, John G.; Riebe, John M.; and Campbell, John P.: The Jet-Augmented Flap. Preprint No. 715, S.M.F. Fund Paper, Inst. Aeronaut. Sci., Jan. 1957.

3. Johnson, Joseph L., Jr.: Wind-Tunnel Investigation of a Small-Scale Sweptback-Wing-Jet-Transport Model Equipped With an External-Flow Jet-Augmented Double Slotted Flap. NASA MEMO 3-8-59L, 1959.

4. Johnson, Joseph L., Jr.: Wind-Tunnel Investigation of the Static Longitudinal Stability and Trim Characteristics of a Sweptback-Wing Jet-Transport Model Equipped With an External-Flow Jet-Augmented Flap. NACA TN 4177, 1958.

5. Fink, Marvin P.: Aerodynamic Characteristics, Temperature, and Noise Measurements of a Large-Scale External-Flow Jet-Augmented-Flap Model With Turbojet Engines Operating. NASA TN D-943, 1961.

6. Parlett, Lysle P.; Fink, Marvin P.; and Freeman, Delma C., Jr. (With appendix B by Marion O. McKinney and Joseph L. Johnson, Jr.): Wind-Tunnel Investigation of a Large Jet Transport Model Equipped With an External-Flow Jet Flap. NASA TN D-4928, 1968.

7. Mechtly, E. A.: The International System of Units – Physical Constants and Conversion Factors. NASA SP-7012, 1964.

8. Chambers, Joseph R.; and Grafton, Sue B.: Static and Dynamic Longitudinal Stability Derivatives of a Powered 1/9-Scale Model of a Tilt-Wing V/STOL Transport. NASA TN D-3591, 1966.

TABLE I.- DIMENSIONS OF MODEL

Wing:	
Area, ft^2 (m^2)	7.87 (0.731)
Span (to theoretical tip), in. (cm)	93.71 (238.02)
Aspect ratio	7.75
Length of mean aerodynamic chord, in. (cm)	13.22 (33.59)
Location of quarter chord of mean aerodynamic chord, referenced to nose of model, in. (cm)	40.54 (102.98)
Spanwise station of mean aerodynamic chord, in. (cm)	19.33 (49.10)
Root chord, in. (cm)	19.49 (49.50)
Tip chord (theoretical tip), in. (cm)	6.54 (16.62)
Break station chord, in. (cm)	12.08 (30.67)
Spanwise station of break station, in. (cm)	20.16 (51.20)
Sweep of quarter-chord line:	
Inboard panel, deg	24.08
Outboard panel, deg	25.00
Dihedral of quarter-chord line:	
Inboard panel, deg	-3.50
Outboard panel, deg	-3.50
Incidence of mean aerodynamic chord, deg	4.50
Incidence of root chord, deg	3.50
Geometric twist:	
Root, deg	0.0
Break station, deg	-1.5
Tip, deg	-3.5
Vertical tail:	
Area, ft^2 (m^2)	1.22 (0.113)
Span, in. (cm)	14.76 (37.48)
Length of mean aerodynamic chord, in. (cm)	11.95 (30.35)
Aspect ratio	1.240
Sweep angles:	
Leading edge, deg	36.6
Trailing edge, deg	29.4
Root chord, in. (cm)	13.22 (33.59)
Tip chord, in. (cm)	10.58 (26.87)
Horizontal tail:	
Area, ft^2 (m^2)	1.73 (0.161)
Span, in. (cm)	35.88 (91.13)
Length of mean aerodynamic chord, in. (cm)	7.28 (18.49)
Location of quarter chord of mean aerodynamic chord, referenced to nose of model, in. (cm)	96.09 (244.06)
Incidence	Variable
Engines:	
Spanwise location of inboard engines, in. (cm)	17.10 (43.43)
Spanwise location of outboard engines, in. (cm)	26.61 (67.58)
Incidence of all engine center lines relative to wing-chord line, deg	-3.00
Moment reference:	
Longitudinal location, referenced to nose of model, in. (cm)	40.54 (102.98)
Vertical location, referenced to top of fuselage at wing, in. (cm)	4.92 (12.49)
Control-surface dimensions:	
Rudder:	
Span, in. (cm)	10.53 (26.75)
Chord, upper end, parallel to water line, in. (cm)	2.67 (6.78)
Chord, lower end, perpendicular to hinge line, in. (cm)	2.72 (6.91)
Hinge-line location, percent chord	75
Sweep of hinge line, deg	31.4
Elevator:	
Span, in. (cm)	13.26 (33.69)
Chord, outboard, in. (cm)	1.27 (3.23)
Chord, inboard, in. (cm)	2.53 (6.43)
Hinge-line location, percent chord	73
Sweep of hinge line, deg	16.5

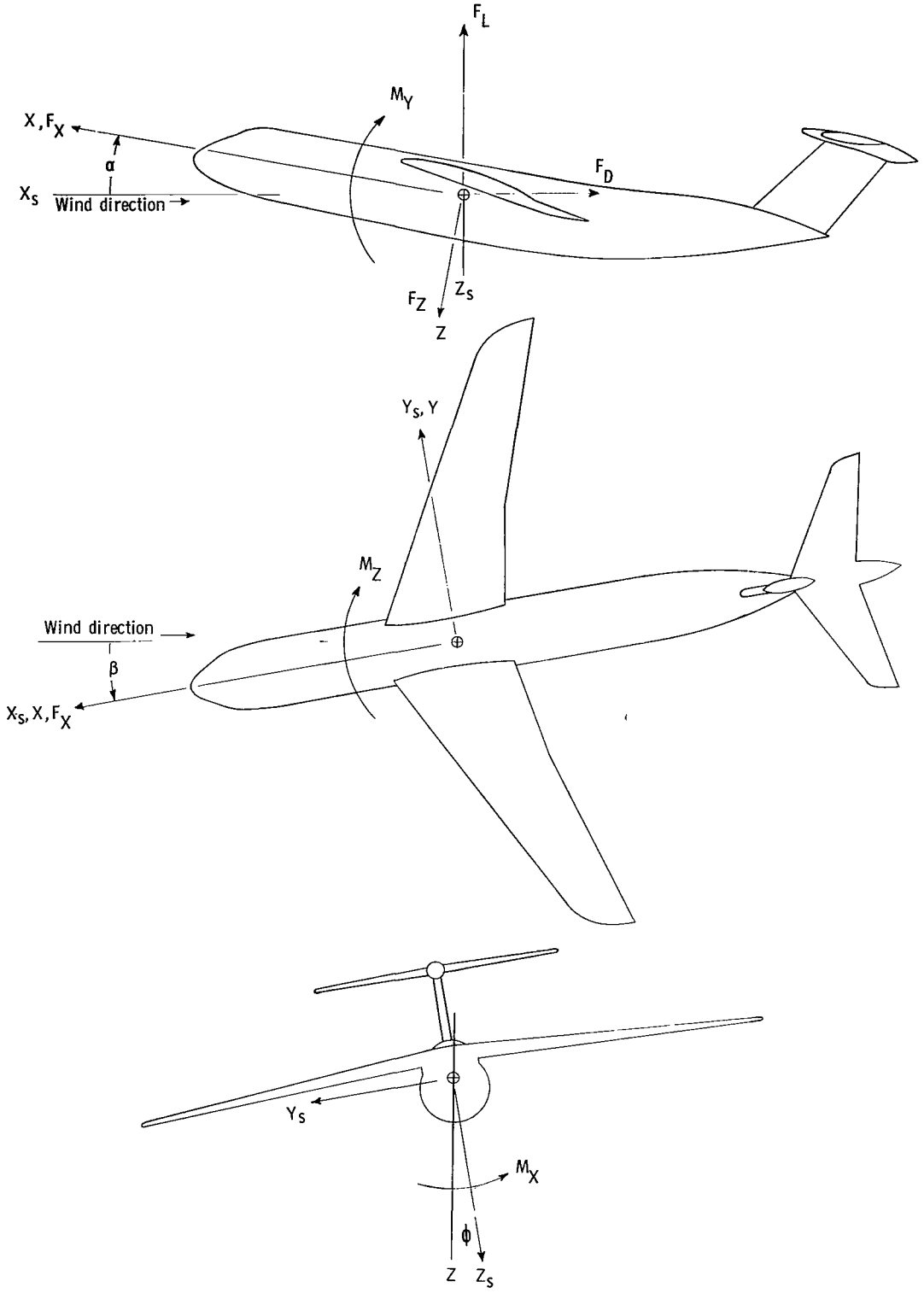

Figure 1.- Axes systems used in presentation of data. Arrows indicate positive direction of moments, axis directions, and angles.

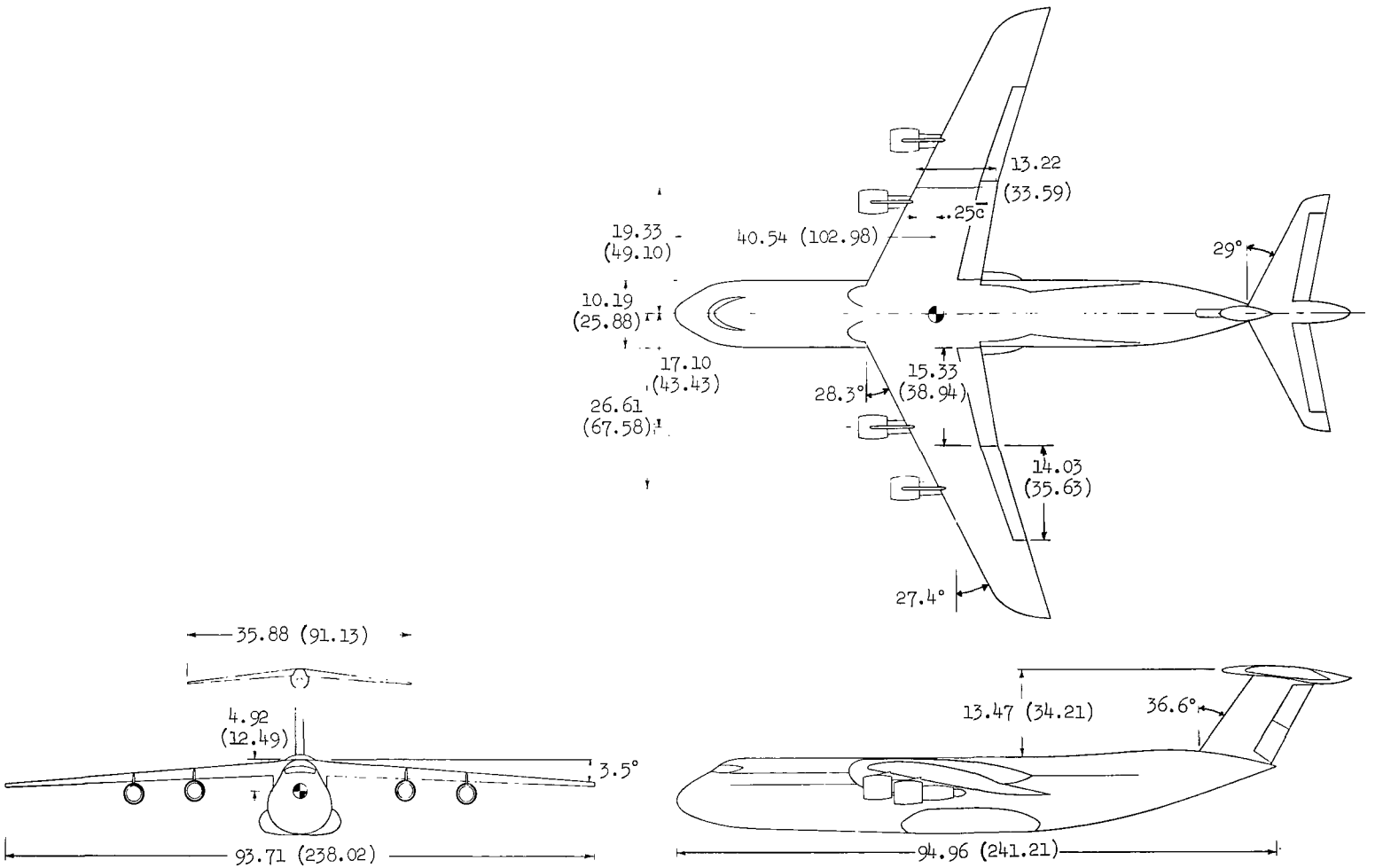

(a) Three-view drawing of complete model.

Figure 2.- Drawing of model used in investigation. All linear dimensions are in inches (centimeters).

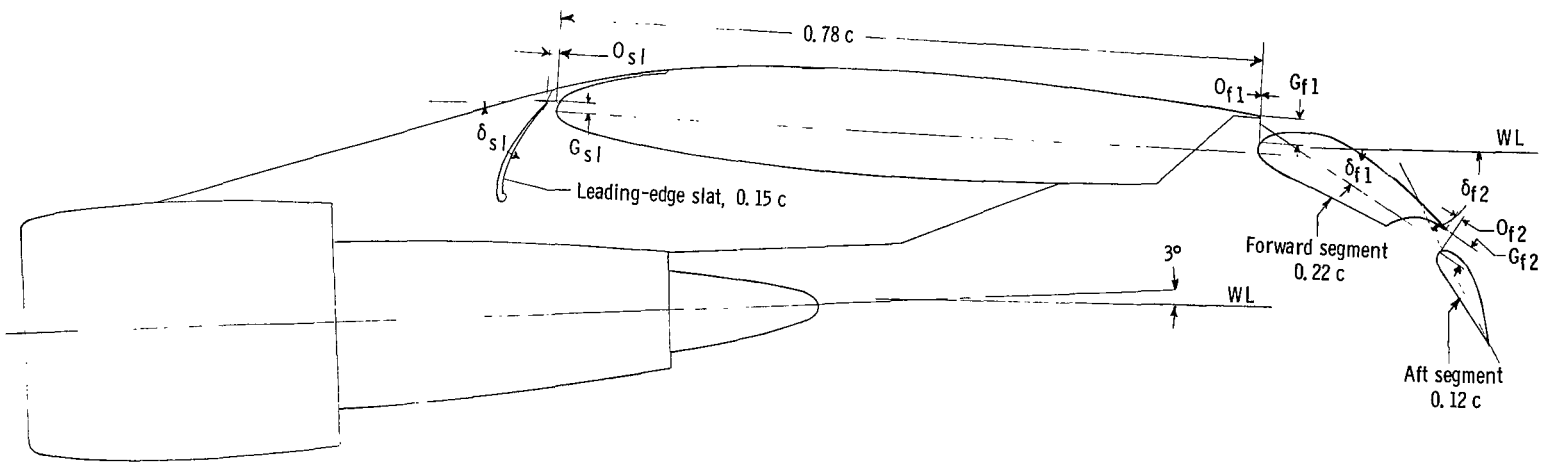

δ_{sl}, deg	Slat gap, G_{sl}, percent c	Slat overlap, O_{sl}, percent c
50	2.5	1
60	2.5	1

δ_{f1}/δ_{f2} deg/deg	Forward-segment gap, G_{f1}, percent c	Forward-segment overlap, O_{f1}, percent c	Aft-segment gap, G_{f2}, percent c	Aft-segment overlap, O_{f2}, percent c
10/20	6.5	0	3.0	0
20/40	5.0	0	2.5	.5
30/60	3.0	0	2.5	.5

(b) Flap assembly and engine-pylon details. (Incidence of thrust line to wing-chord line may be obtained in table I.)

Figure 2.- Concluded.

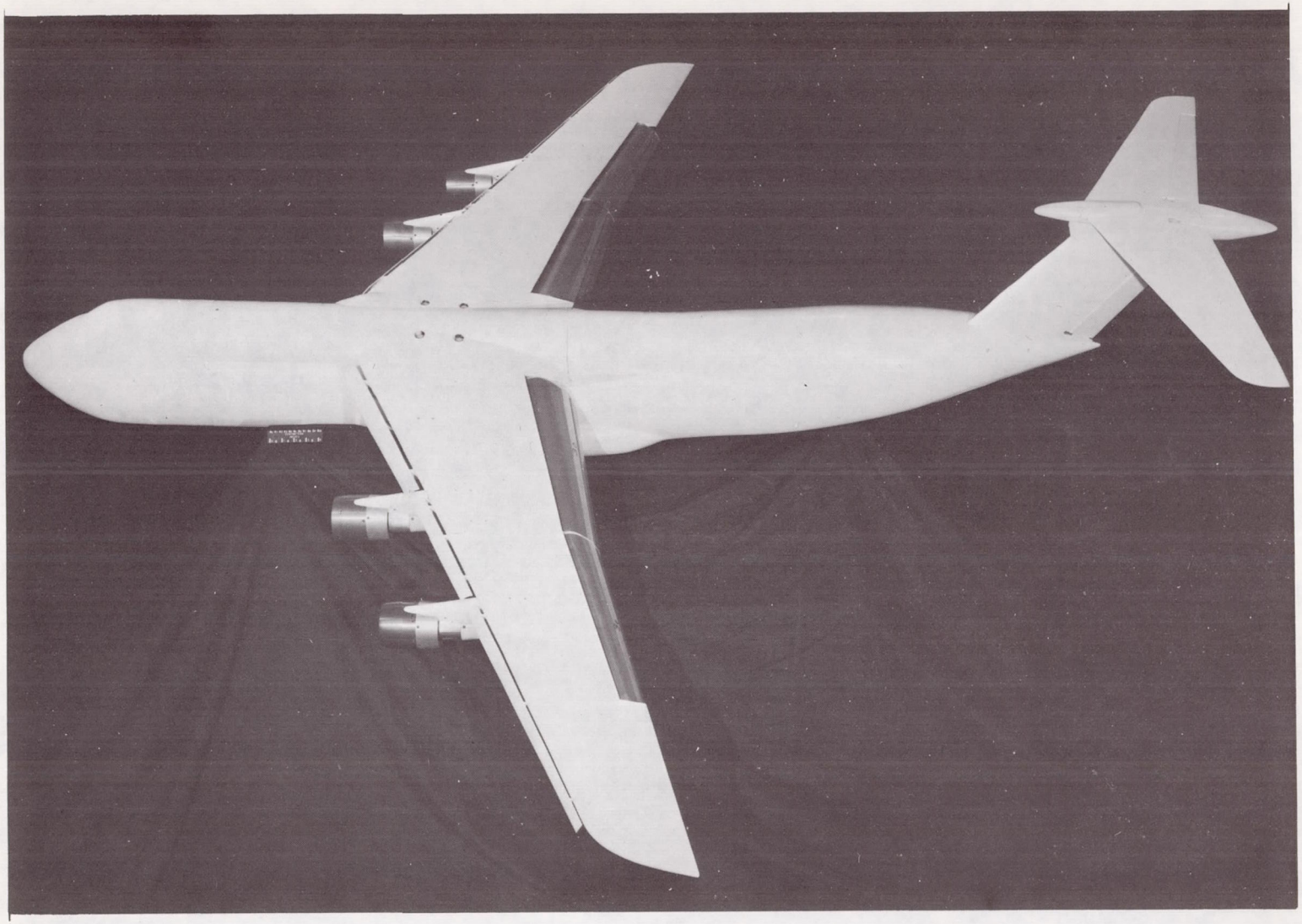

(a) Top view of model. L-68-8093

Figure 3.- Photographs of model and flap system.

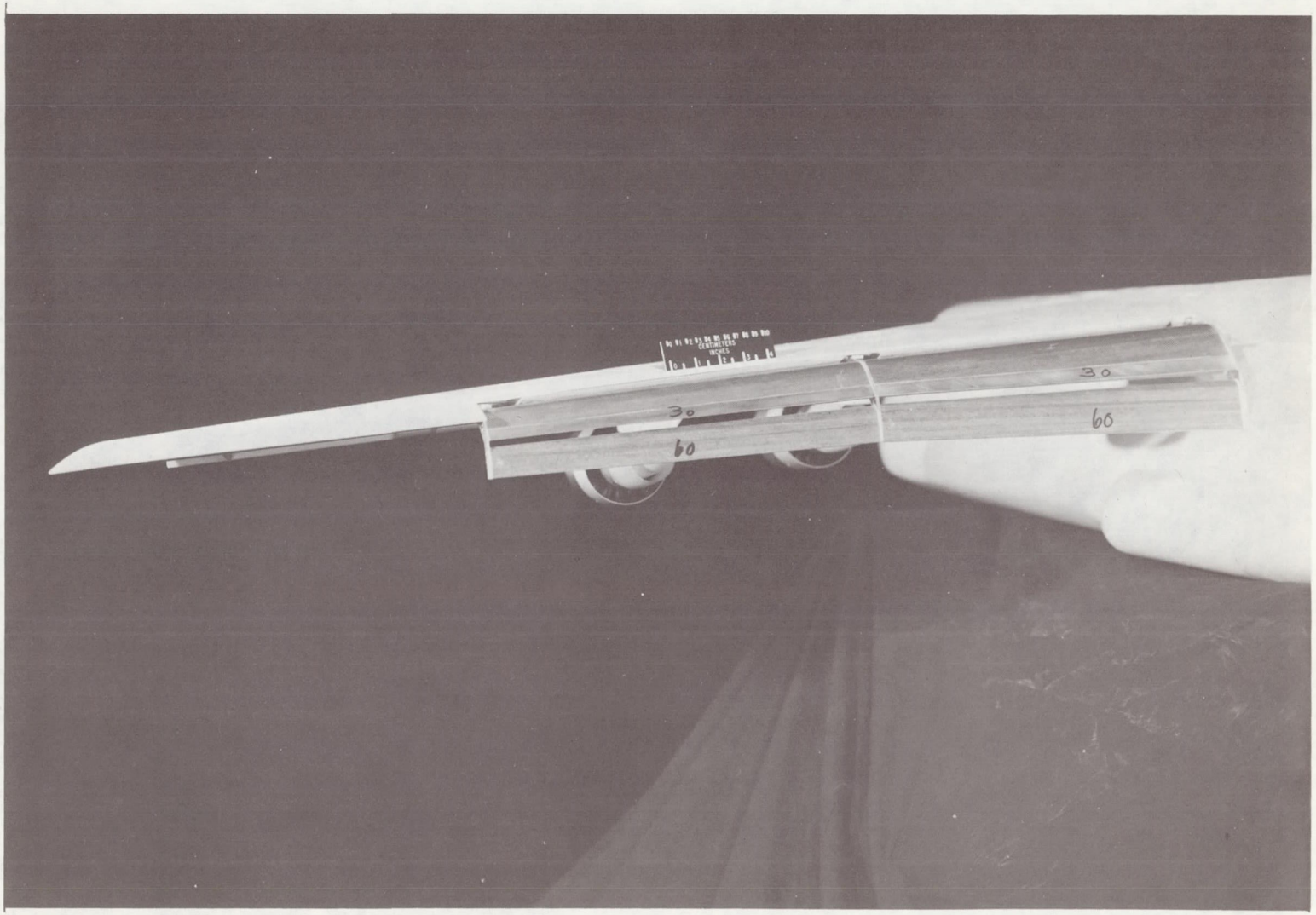

(b) Flap system.

L-68-8094

Figure 3.- Concluded.

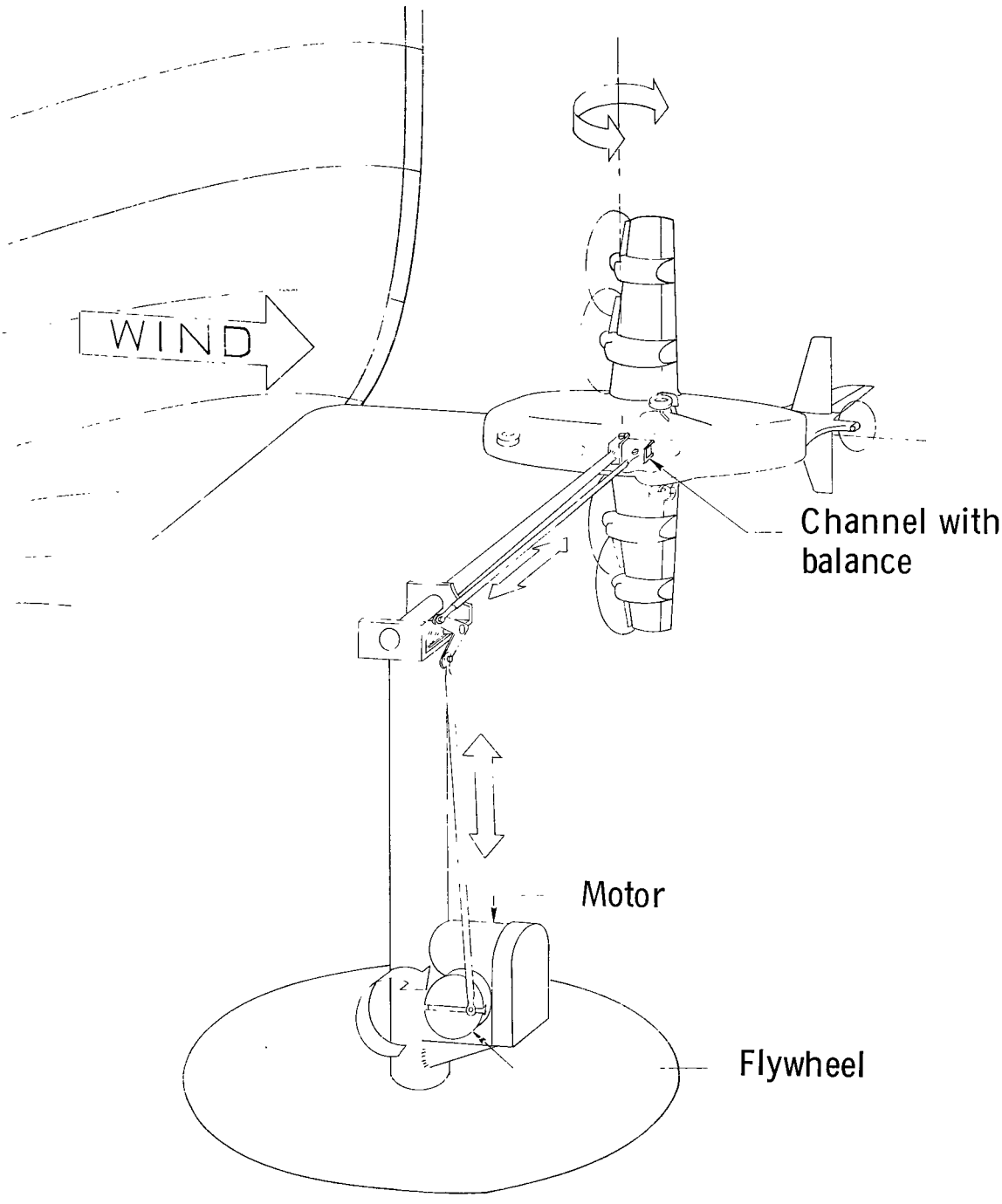

(a) Pitching setup.

Figure 4.- Sketches of test setup for oscillatory force tests.

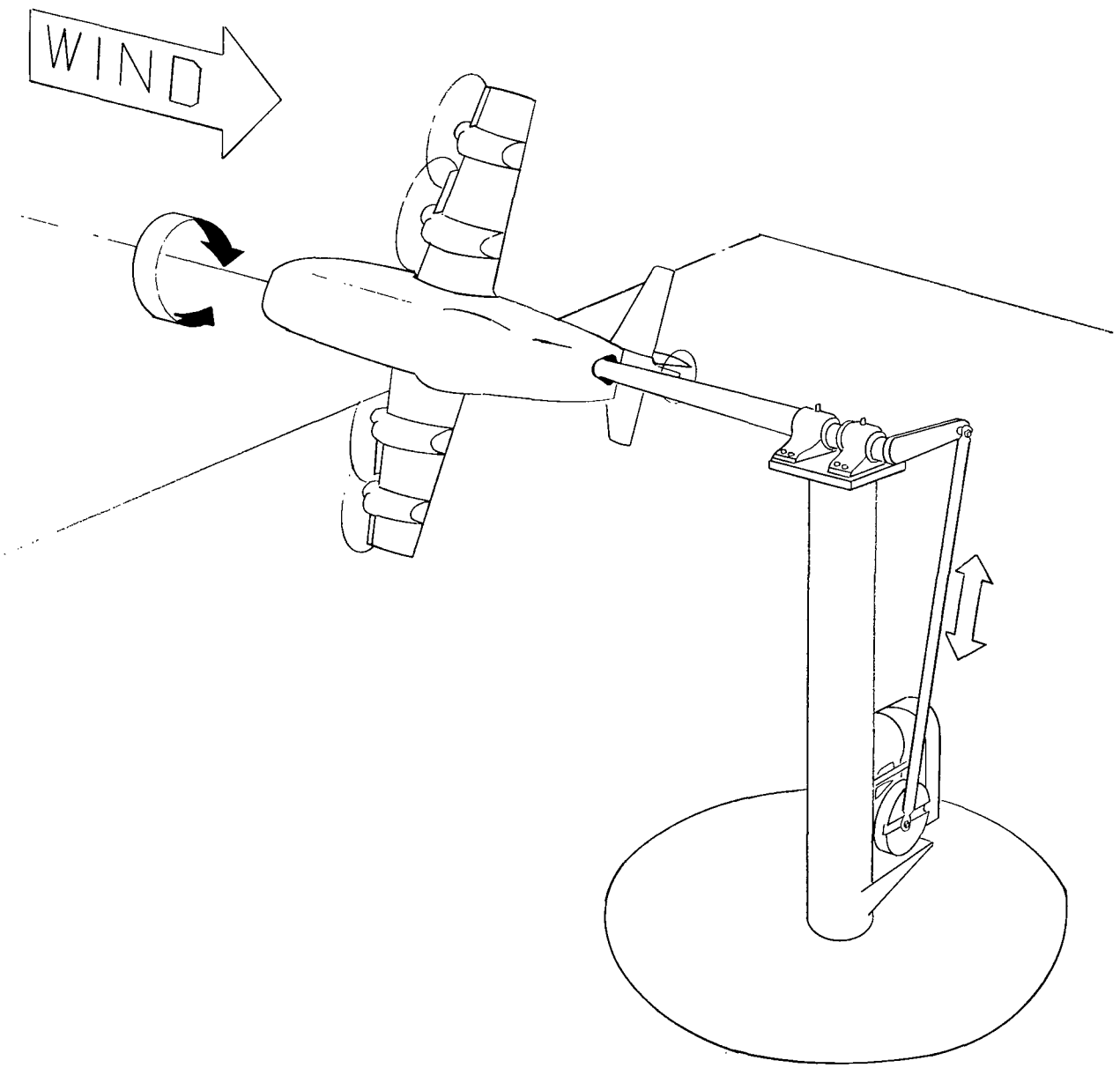

(b) Rolling setup.

Figure 4.- Continued.

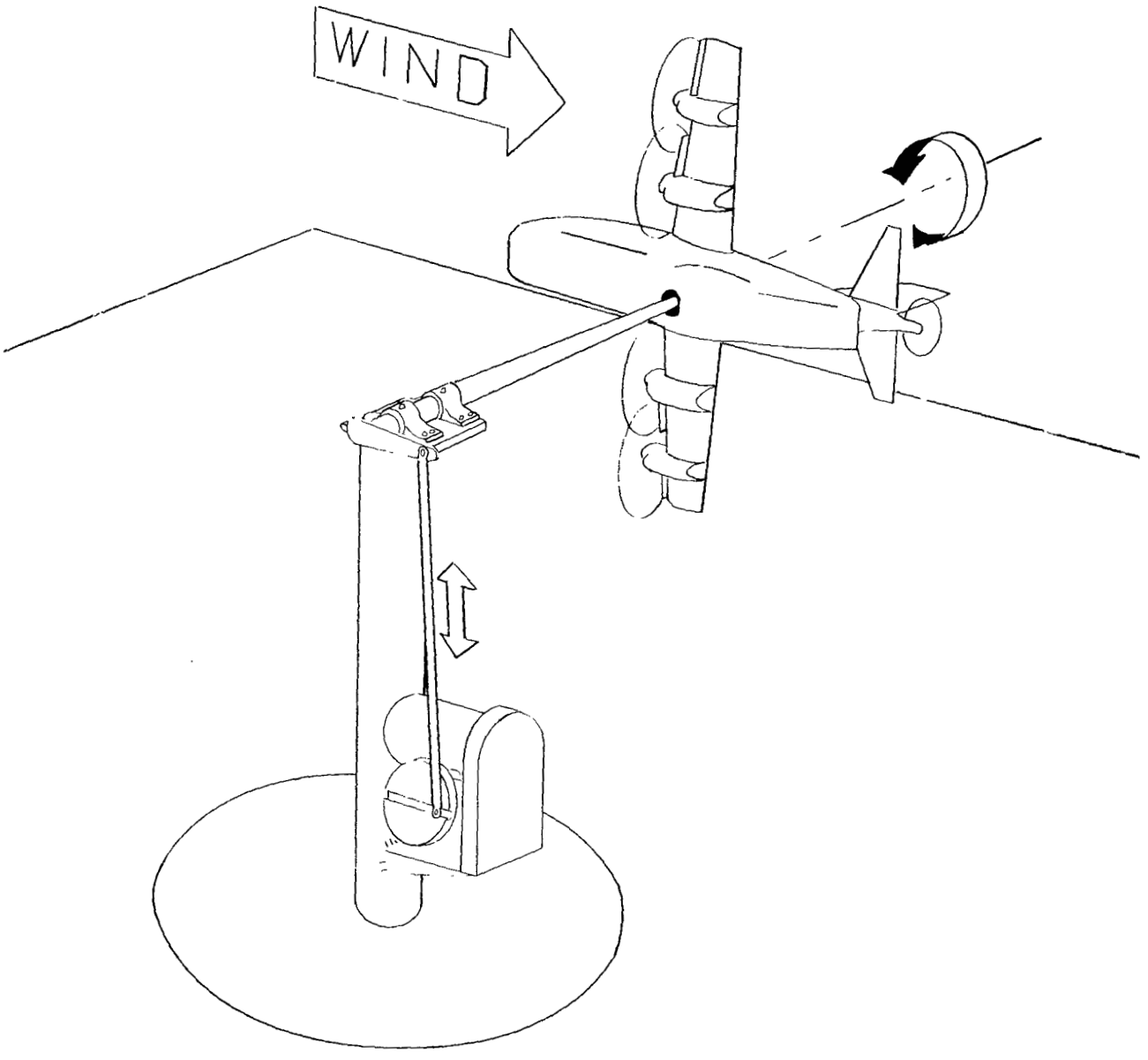

(c) Yawing setup.

Figure 4.- Concluded.

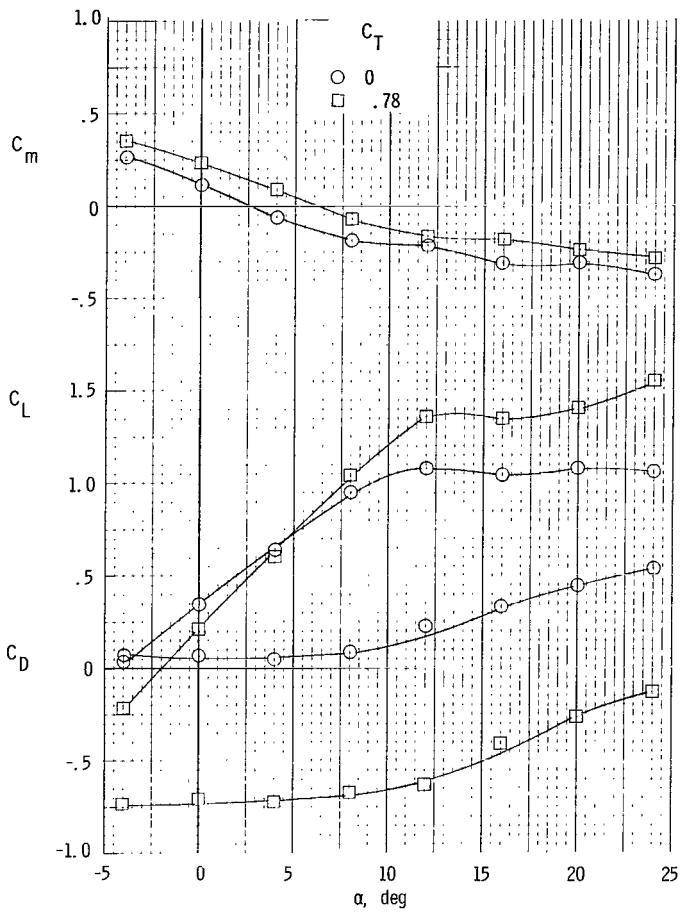

(a) $\delta_{f1}/\delta_{f2} = 0^o/0^o$; $i_t = 0^o$; $\delta_e = 0^o$; $\delta_{sl} = 0^o$.

Figure 5.- Effect of power on static longitudinal stability derivatives.

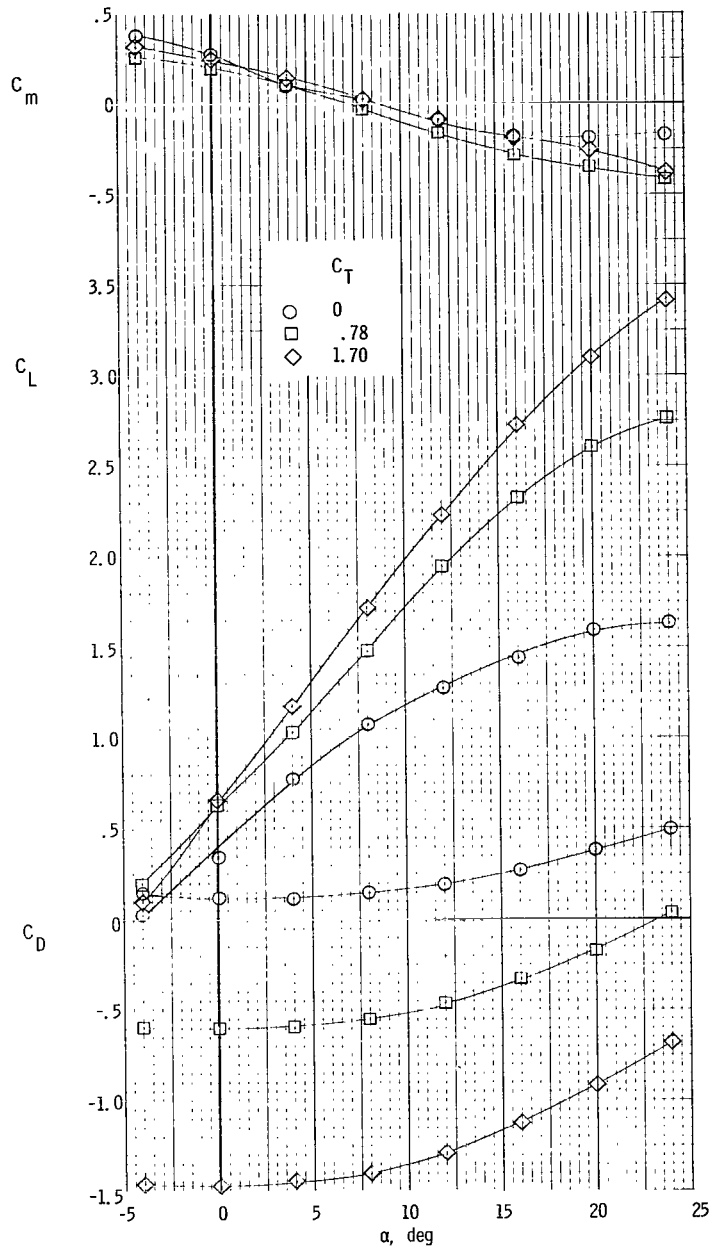

(b) $\delta_{f1}/\delta_{f2} = 10^0/20^0$; $i_t = 0^0$; $\delta_e = -10^0$; $\delta_{sl} = 50^0$.

Figure 5.- Continued.

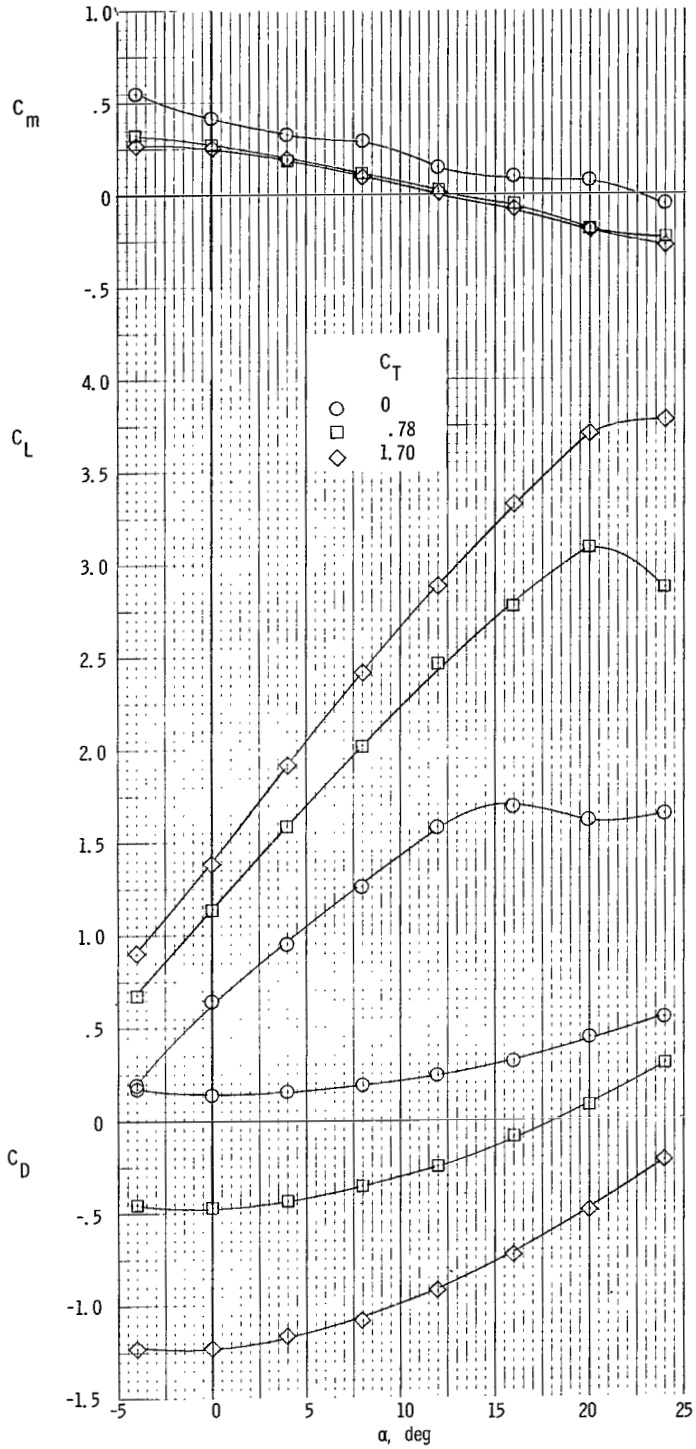

(c) $\delta_{f1}/\delta_{f2} = 20^0/40^0$; $i_t = -5^0$; $\delta_e = -10^0$; $\delta_{sl} = 50^0$.

Figure 5.- Continued.

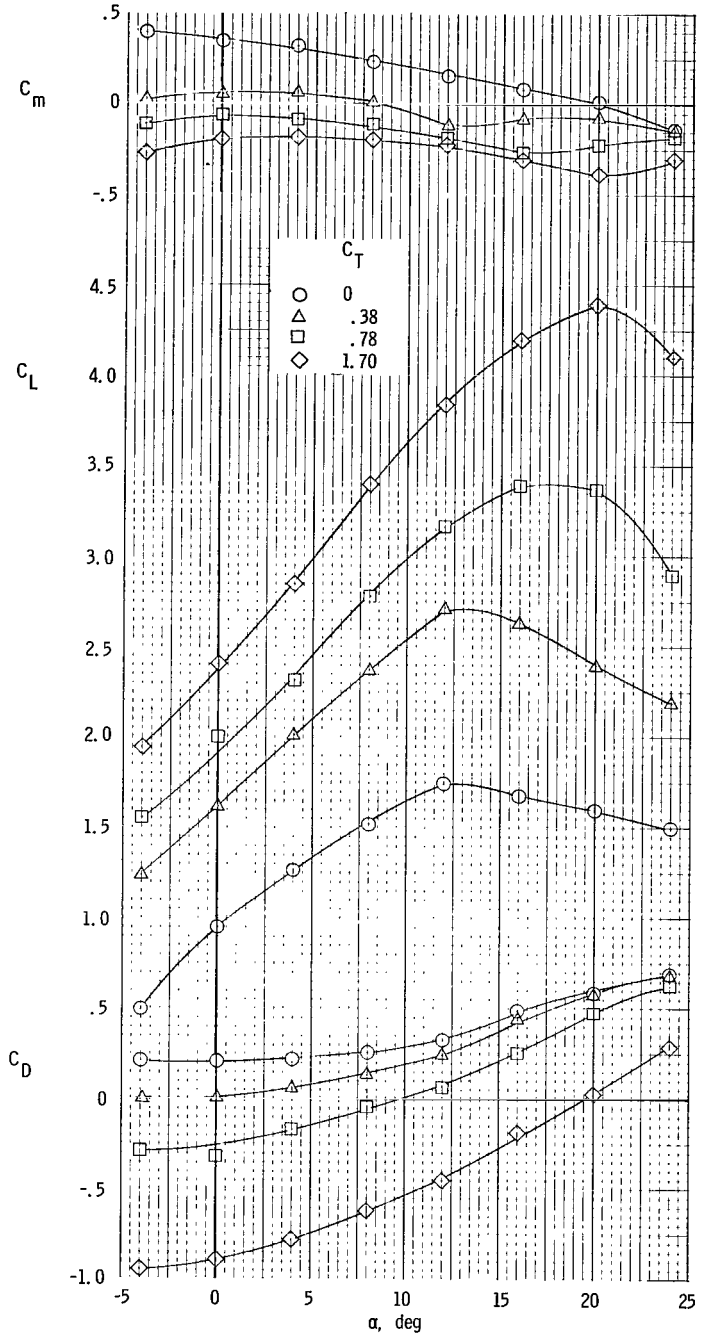

(d) $\delta_{f1}/\delta_{f2} = 30^0/60^0$; $i_t = -9^0$; $\delta_e = 0^0$; $\delta_{sl} = 60^0$.

Figure 5.- Concluded.

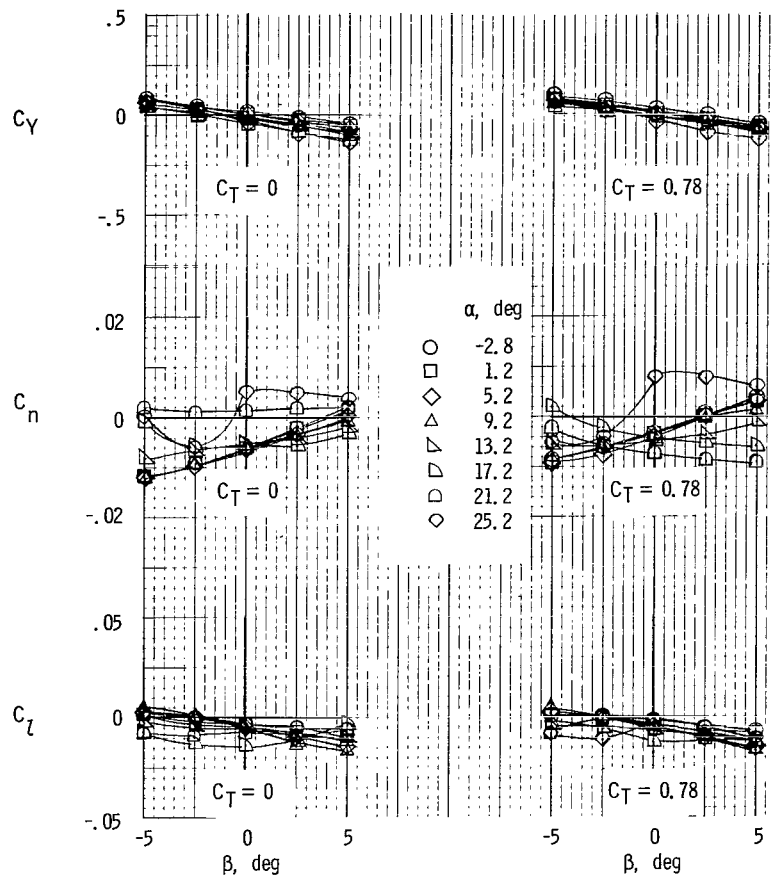

(a) $\delta_{f1}/\delta_{f2} = 0^o/0^o$; $i_t = 0^o$; $\delta_e = 0^o$; $\delta_{sl} = 0^o$.

Figure 6.- Static lateral stability derivatives of model.

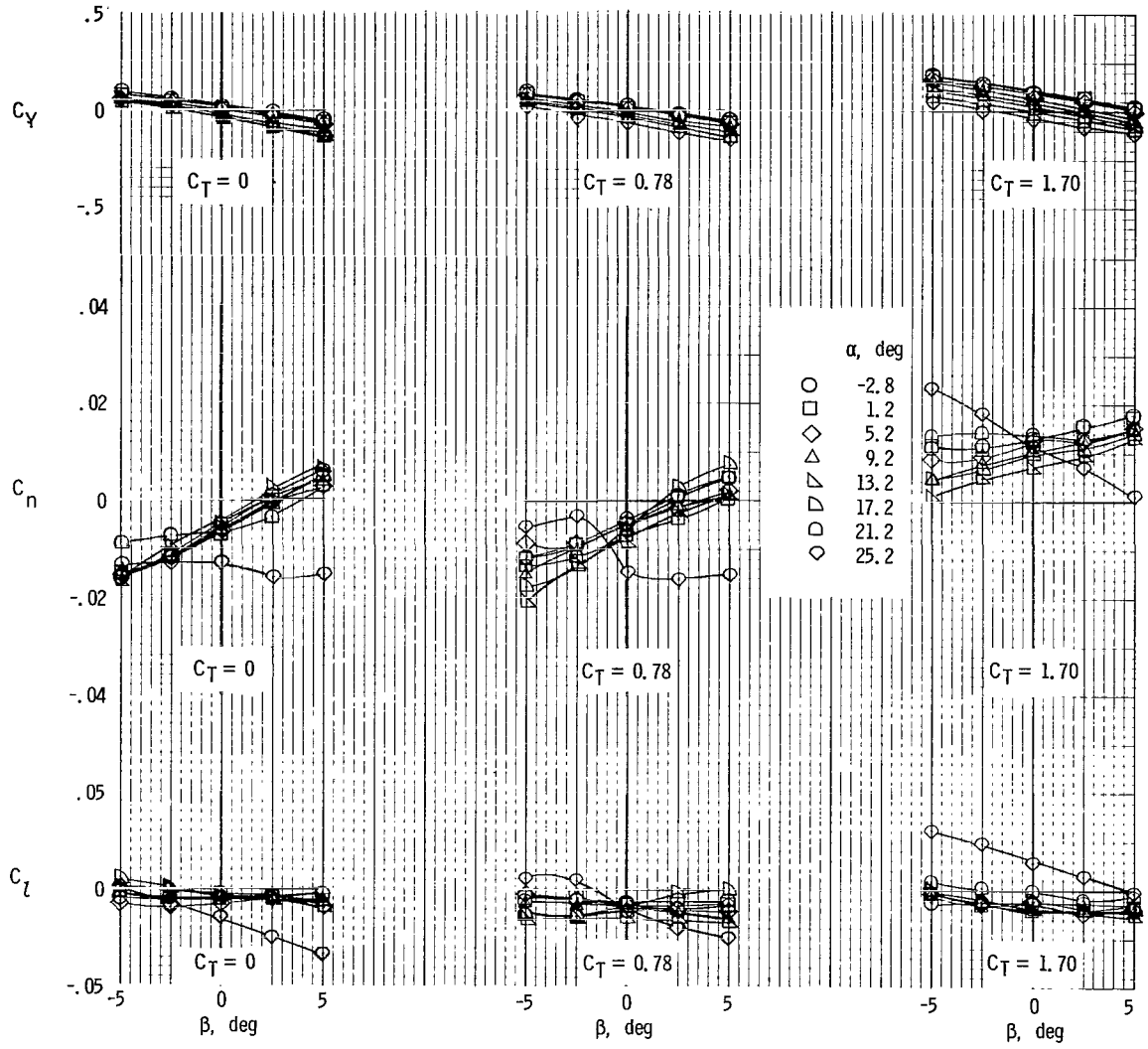

(b) $\delta_{f1}/\delta_{f2} = 20^0/40^0$; $i_t = 0^0$; $\delta_e = -10^0$; $\delta_{sl} = 50^0$.

Figure 6.- Continued.

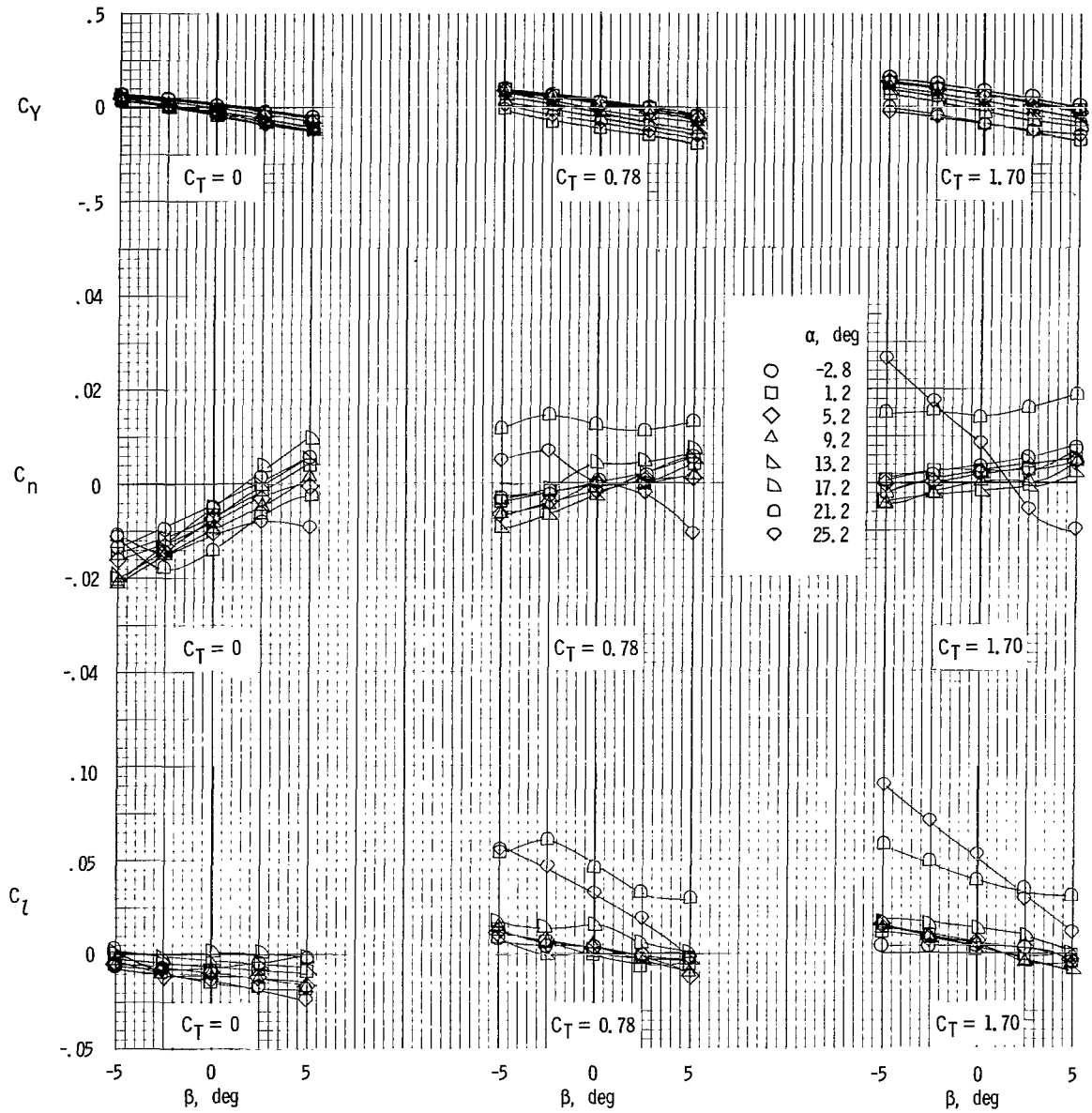

(c) $\delta_{f1}/\delta_{f2} = 10^0/20^0$; $i_t = -5^0$; $\delta_e = -10^0$; $\delta_{sl} = 50^0$.

Figure 6.- Continued.

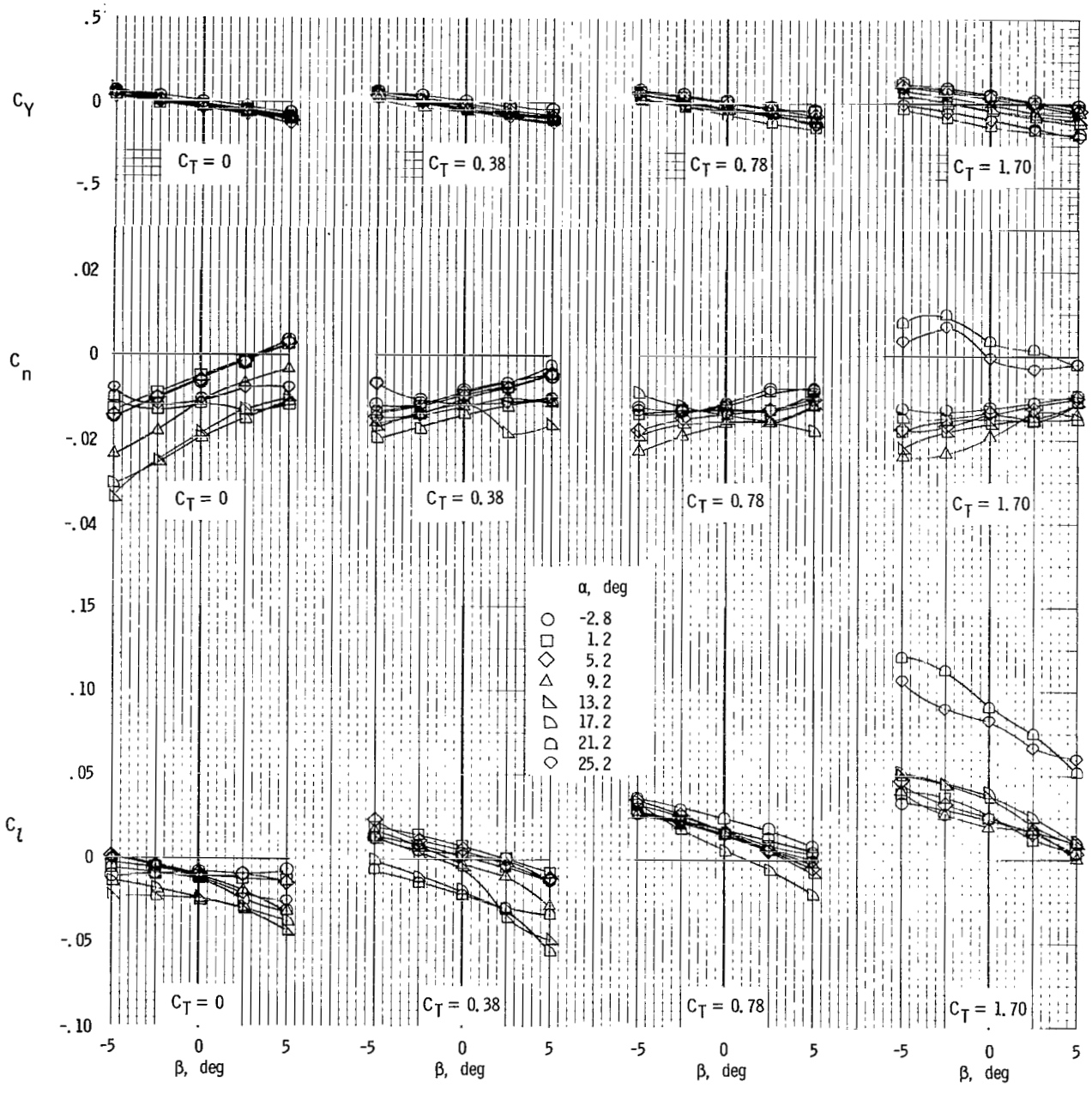

(d) $\delta_{f1}/\delta_{f2} = 30^0/60^0$; $i_t = -9^0$; $\delta_e = 0^0$; $\delta_{sl} = 60^0$.

Figure 6.- Concluded.

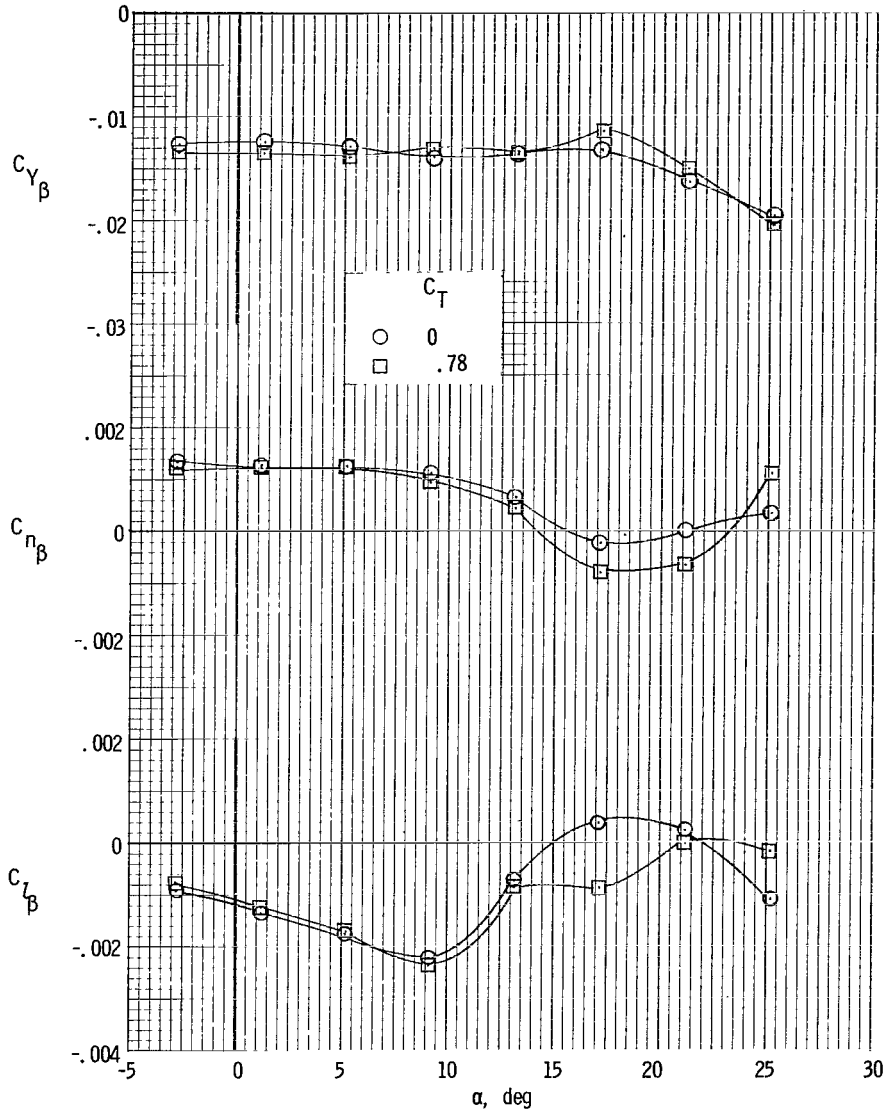

(a) $\delta_{f1}/\delta_{f2} = 0^0/0^0$; $i_t = 0^0$; $\delta_e = 0^0$; $\delta_{sl} = 0^0$.

Figure 7.- Static lateral-stability parameters of model with respect to angle of attack.

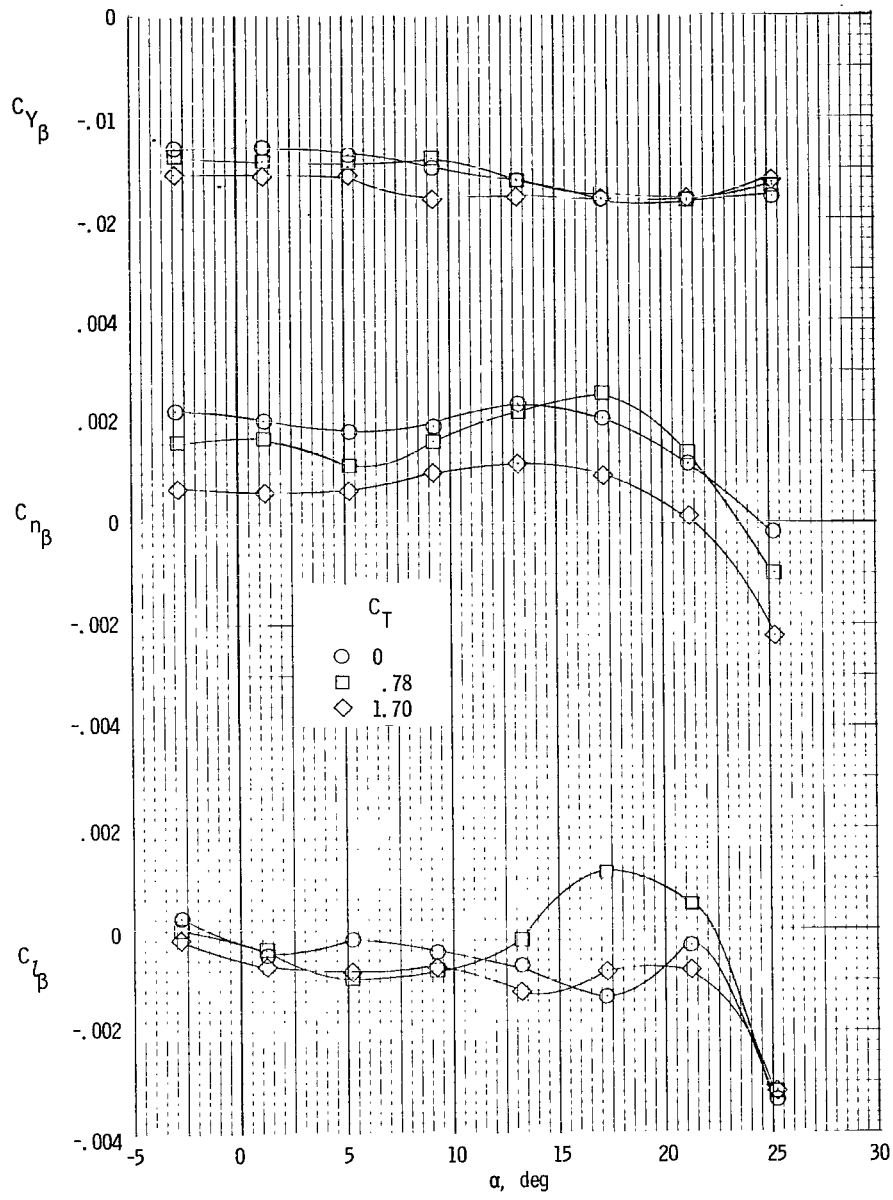

(b) $\delta_{f1}/\delta_{f2} = 10^o/20^o$; $i_t = 0^o$; $\delta_e = -10^o$; $\delta_{sl} = 50^o$.

Figure 7.- Continued.

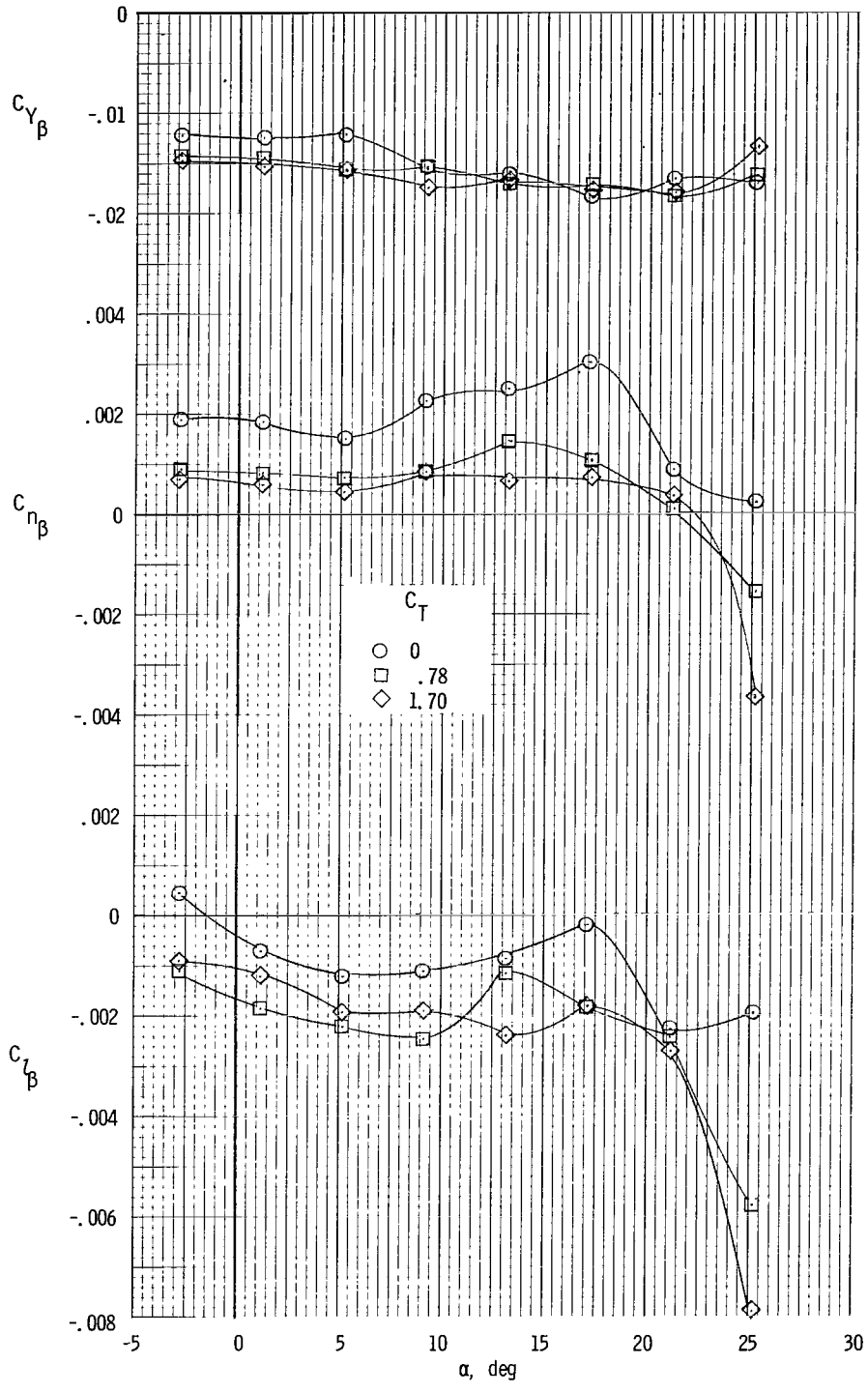

(c) $\delta_{f1}/\delta_{f2} = 20^0/40^0$; $i_t = -5^0$; $\delta_e = -10^0$; $\delta_{sl} = 50^0$.

Figure 7.- Continued.

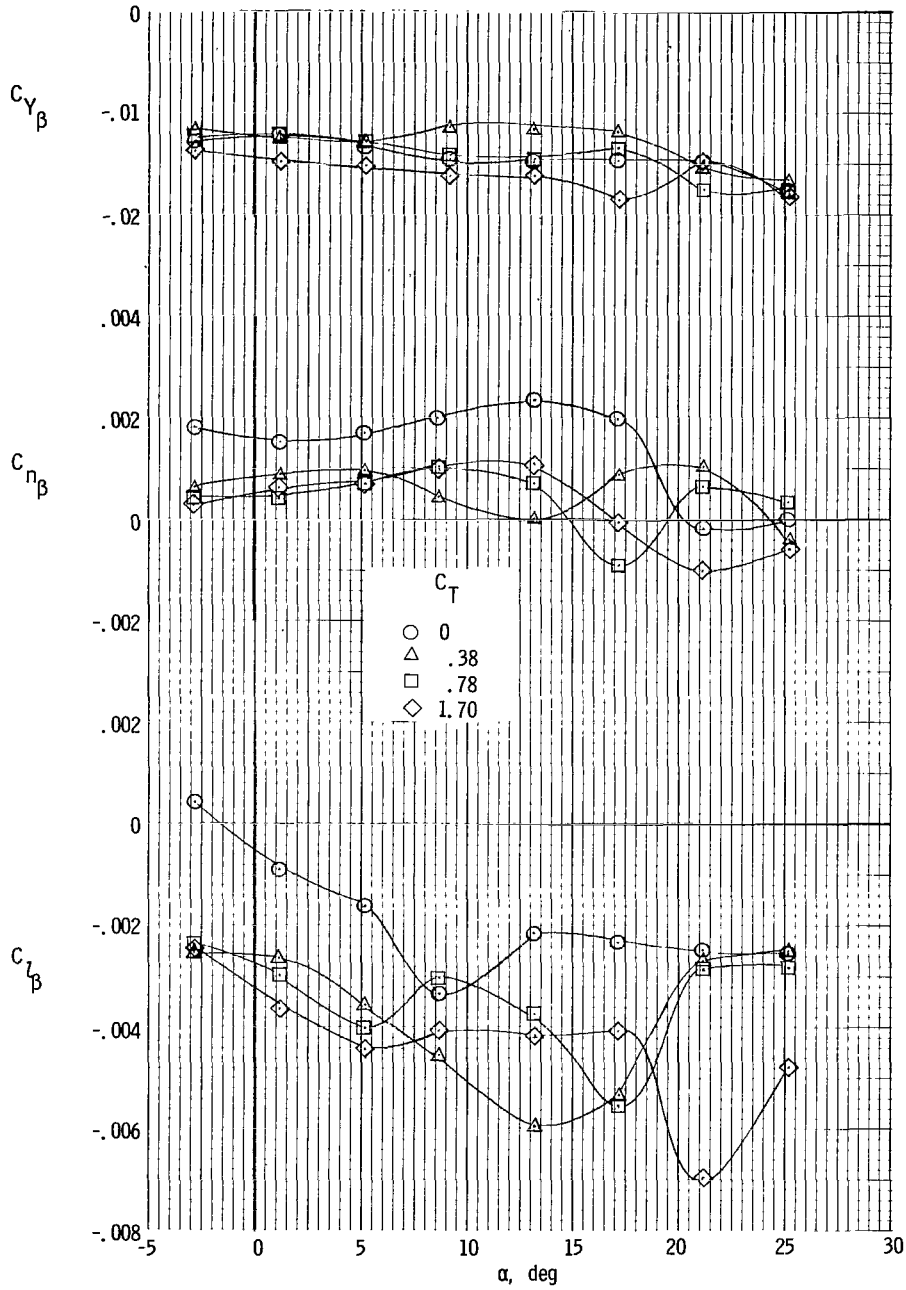

(d) $\delta_{f1}/\delta_{f2} = 30^0/60^0$; $i_t = -9^0$; $\delta_e = 0^0$; $\delta_{sl} = 60^0$.

Figure 7.- Concluded.

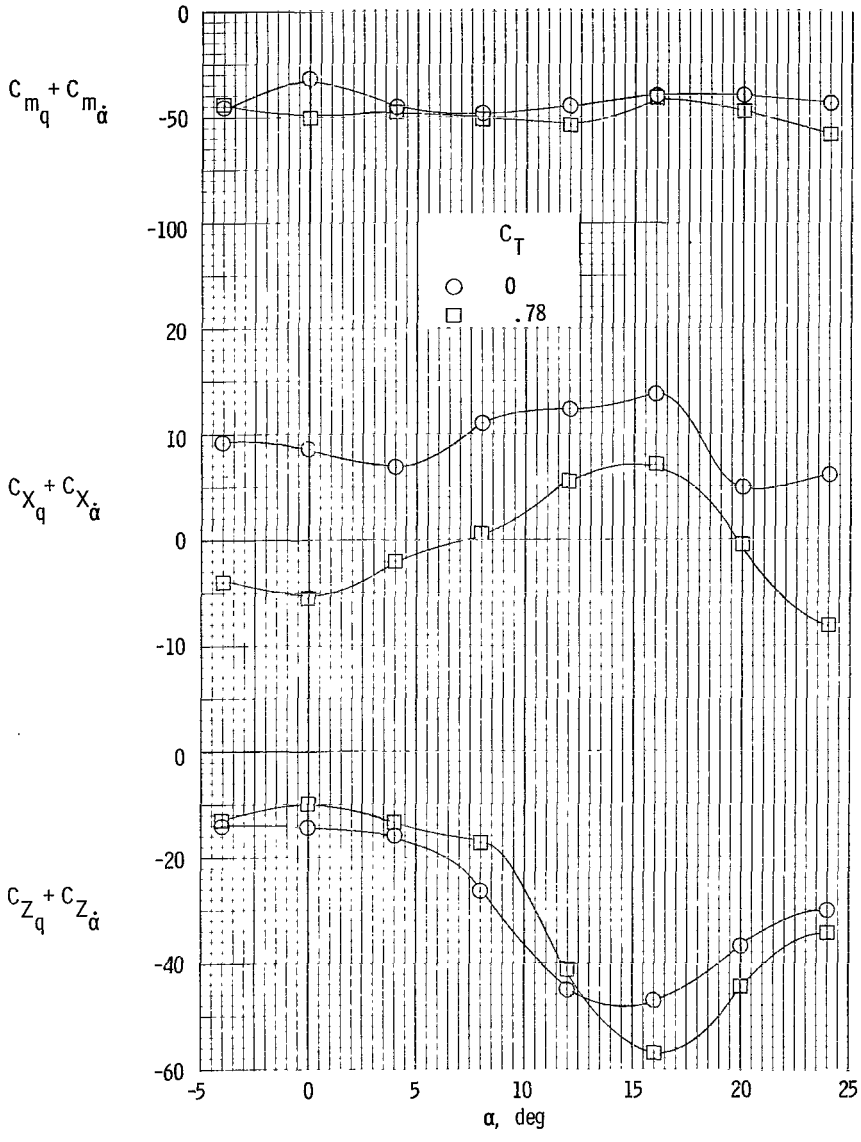

(a) $\delta_{f1}/\delta_{f2} = 0^0/0^0$; $i_t = 0^0$; $\delta_e = 0^0$; $\delta_{sl} = 0^0$.

Figure 8.- Variation of oscillatory pitching derivatives with angle of attack k = 0.045.

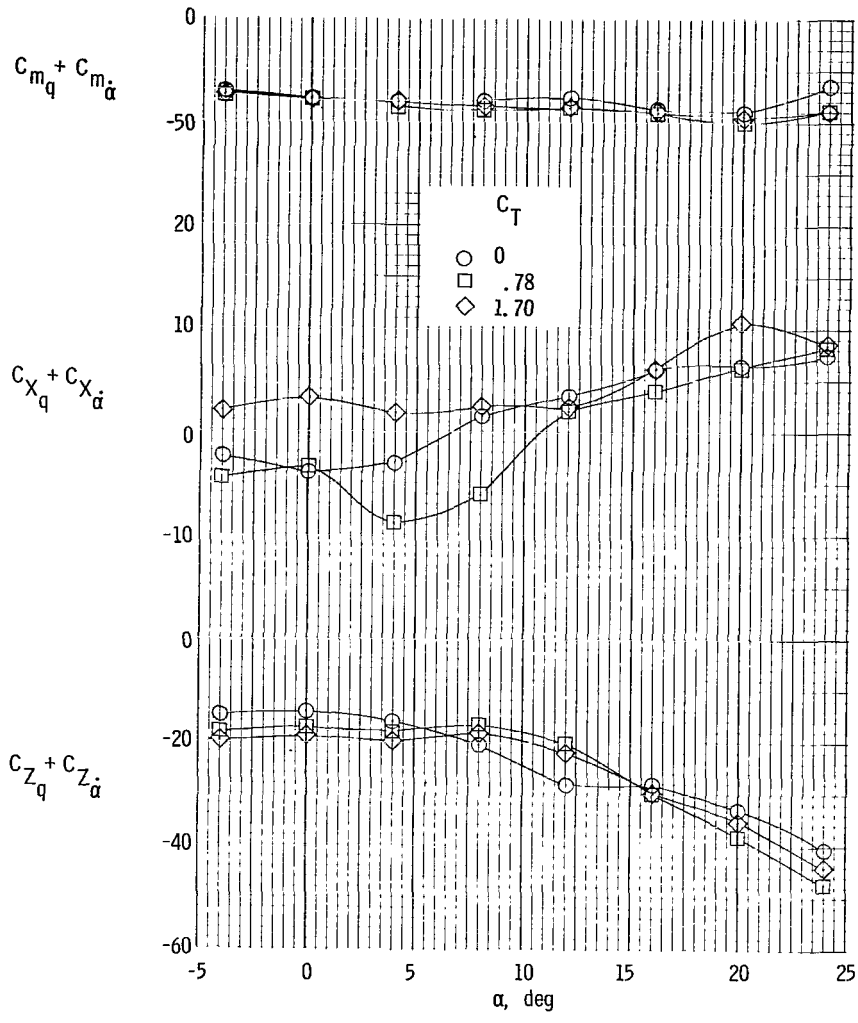

(b) $\delta_{f1}/\delta_{f2} = 10^0/20^0$; $i_t = 0^0$; $\delta_e = -10^0$; $\delta_{sl} = 50^0$.

Figure 8.- Continued.

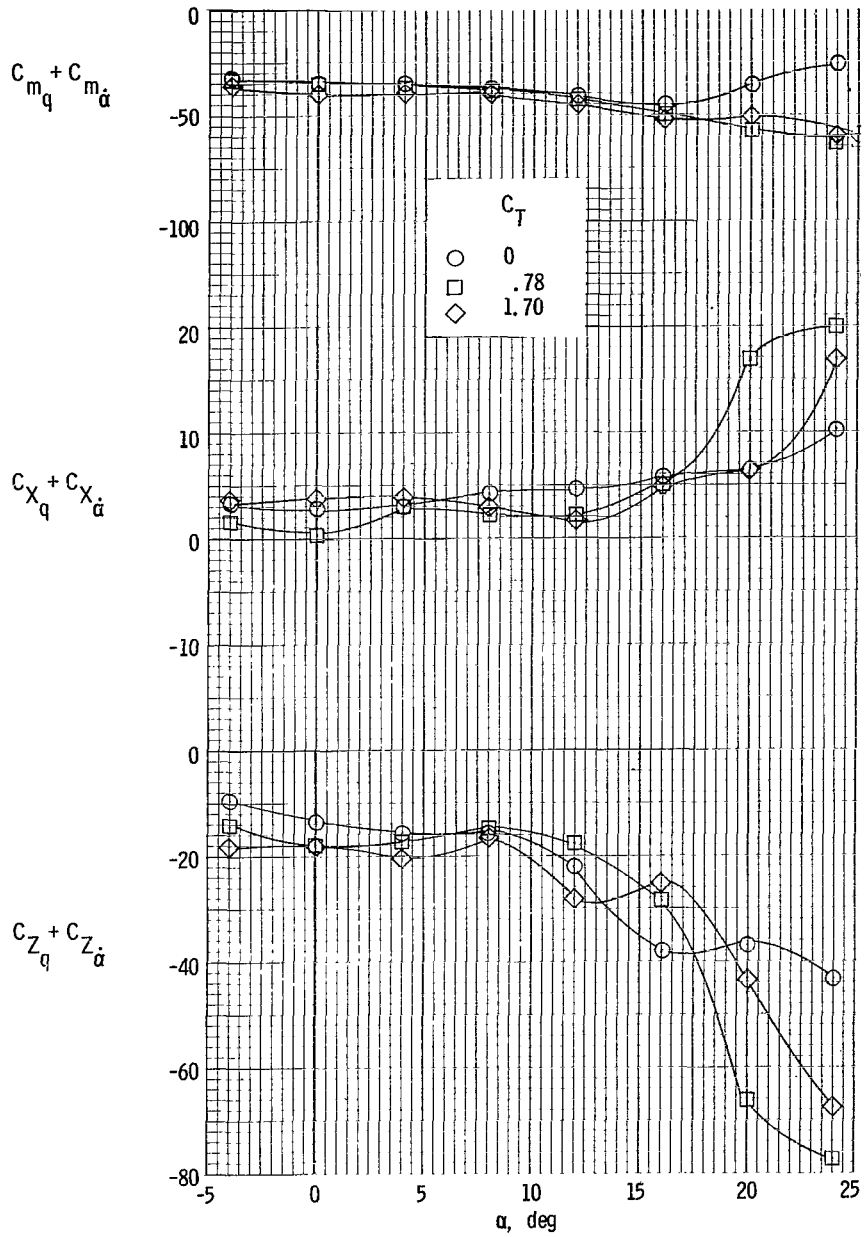

(c) $\delta_{f1}/\delta_{f2} = 20^o/40^o$; $i_t = -5^o$; $\delta_e = -10^o$; $\delta_{sl} = 50^o$.

Figure 8.- Continued.

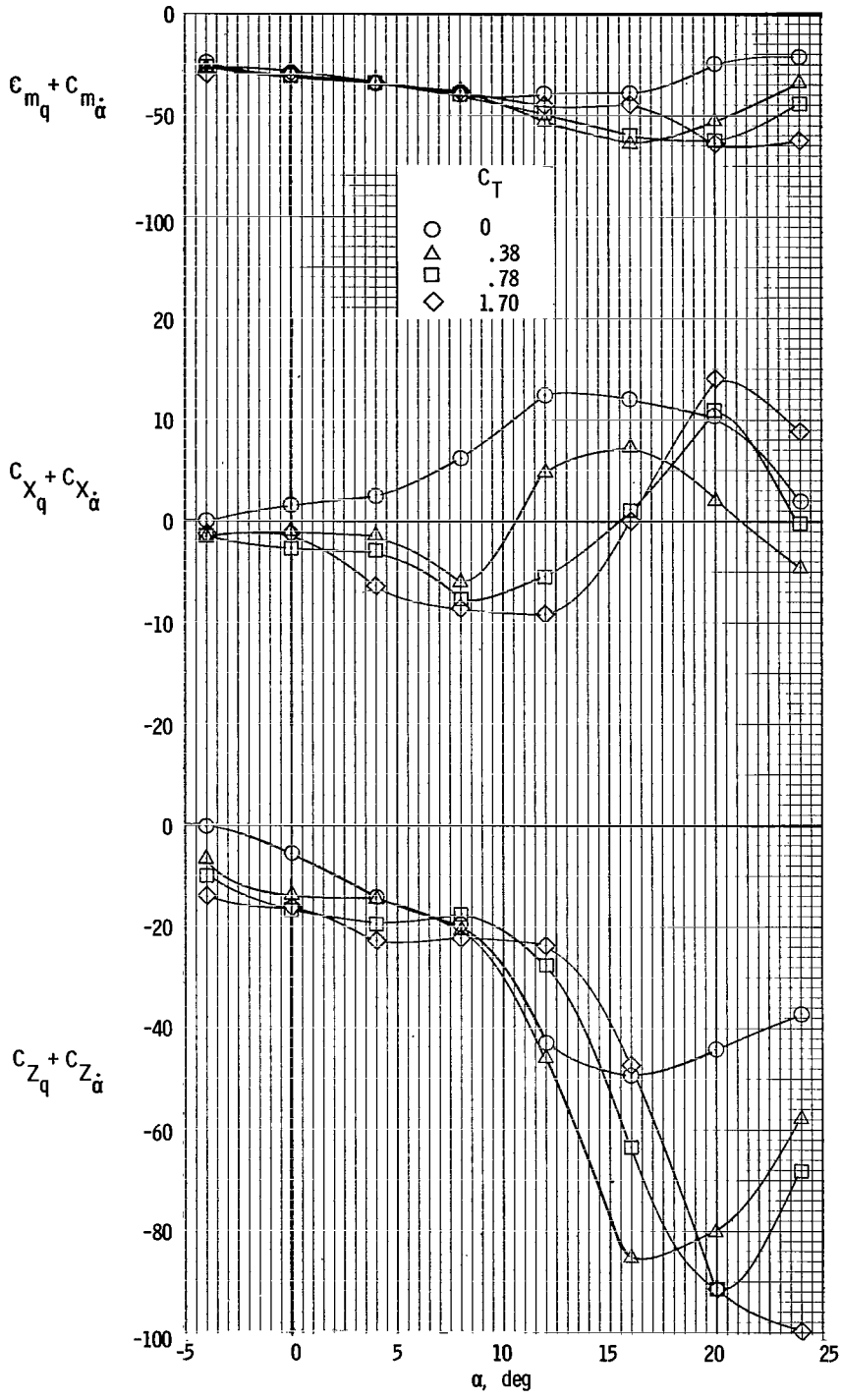

(d) $\delta_{f1}/\delta_{f2} = 30^0/60^0$; $i_t = -9^0$; $\delta_e = 0^0$; $\delta_{sl} = 60^0$.

Figure 8.- Concluded.

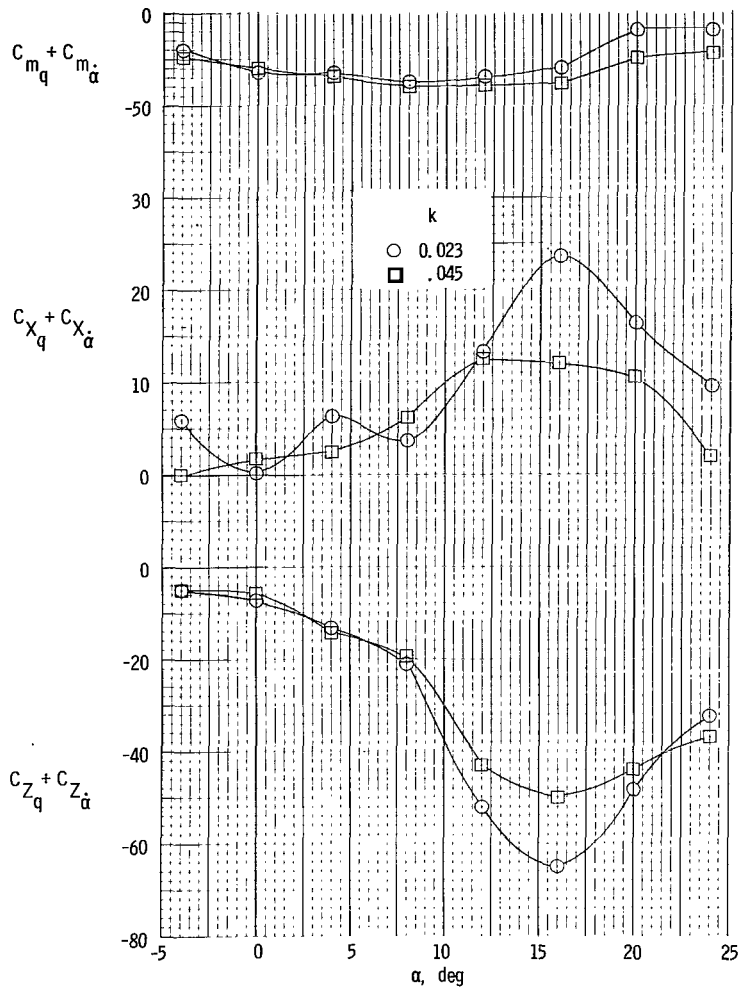

(a) $C_T = 0$.

Figure 9.- Effect of frequency on dynamic pitching derivatives. $\delta_{f1}/\delta_{f2} = 30^0/60^0$; $i_t = -9^0$; $\delta_e = 0^0$; $\delta_{sl} = 60^0$.

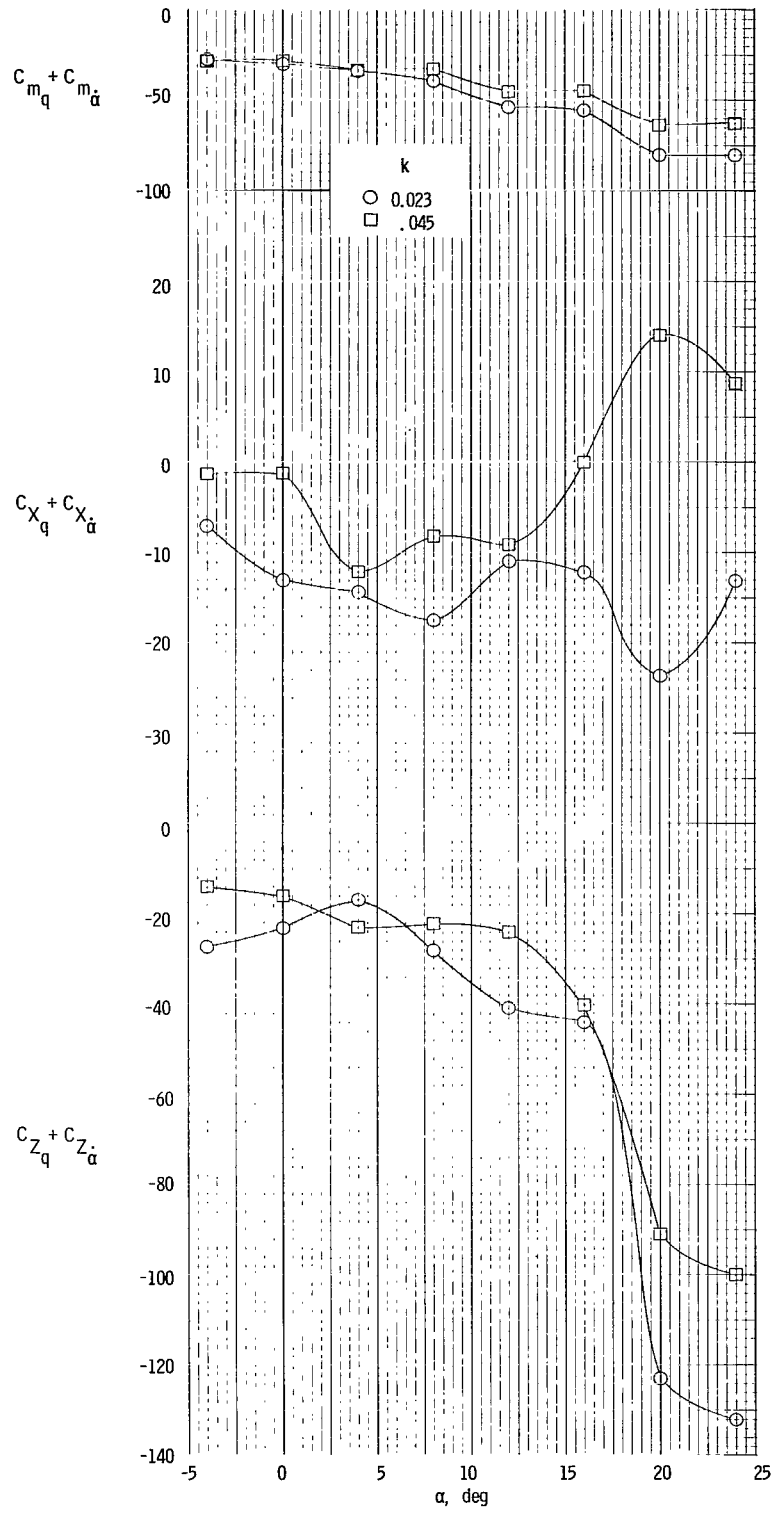

(b) $C_T = 1.70$.

Figure 9.- Concluded.

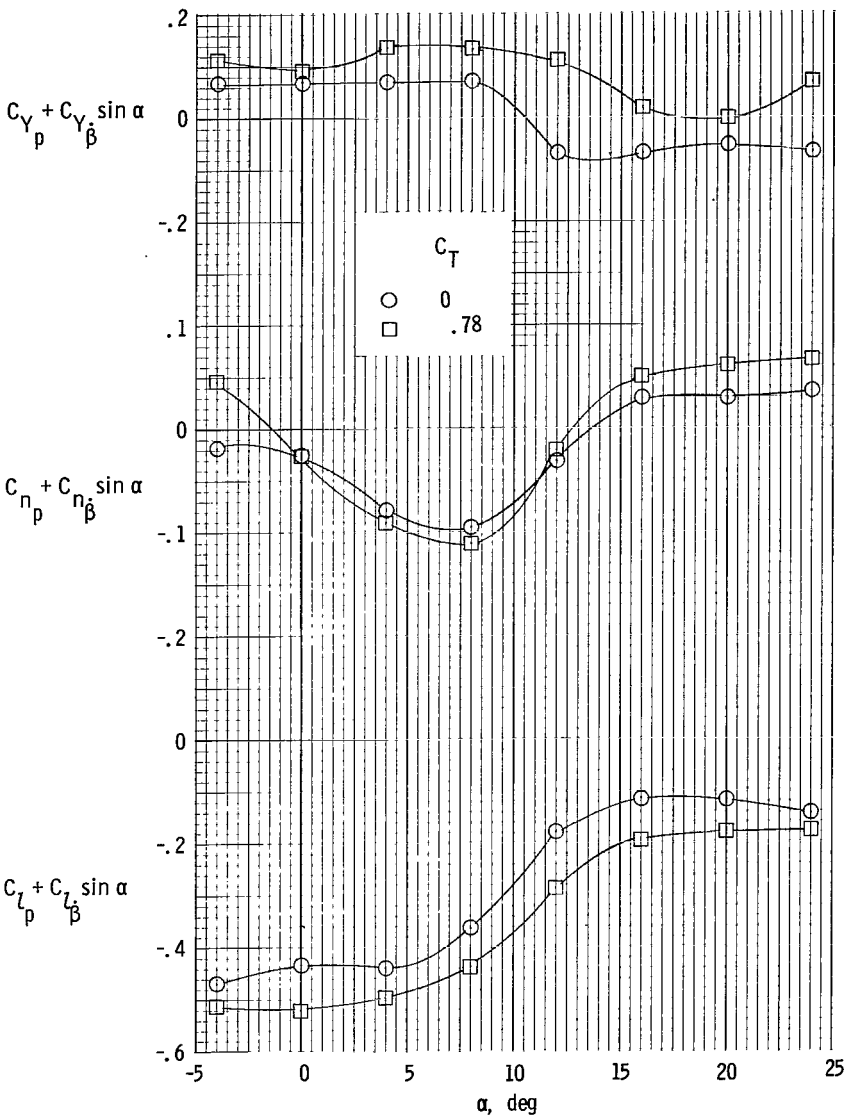

(a) $\delta_{f1}/\delta_{f2} = 0^0/0^0$; $i_t = 0^0$; $\delta_e = 0^0$; $\delta_{sl} = 0^0$.

Figure 10.- Variation of lateral oscillatory rolling derivatives with angle of attack. k = 0.321.

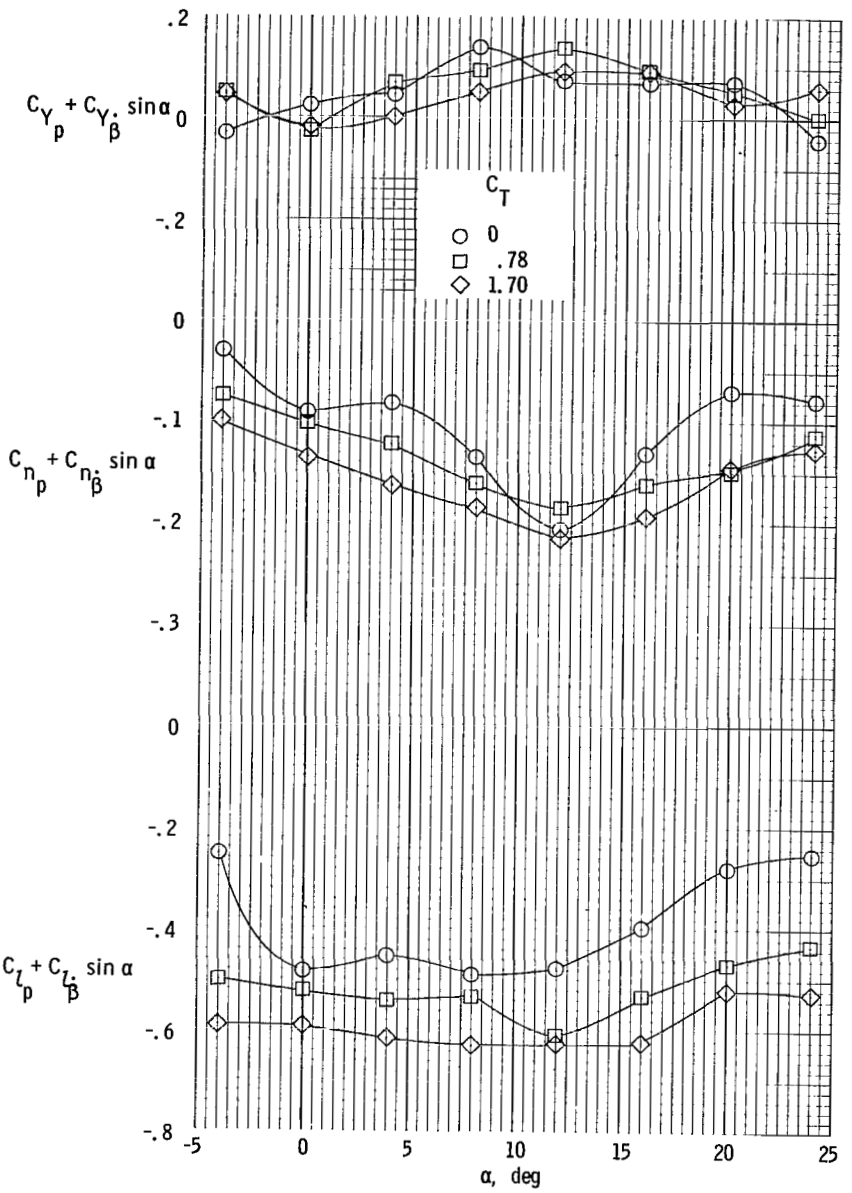

(b) $\delta_{f1}/\delta_{f2} = 10^0/20^0$; $i_t = 0^0$; $\delta_e = -10^0$; $\delta_{sl} = 50^0$.

Figure 10.- Continued.

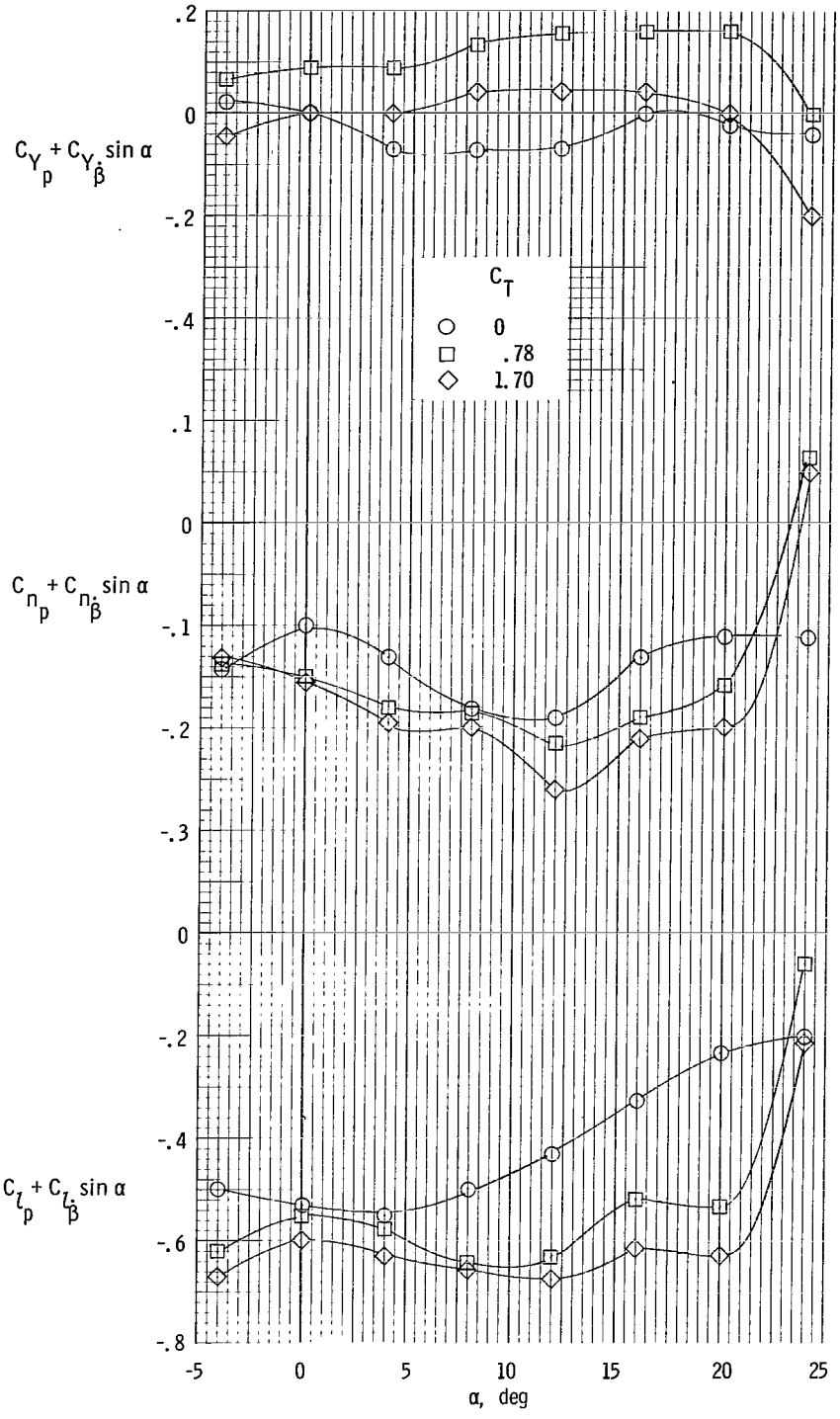

(c) $\delta_{f1}/\delta_{f2} = 20^0/40^0$; $i_t = -5^0$; $\delta_e = -10^0$; $\delta_{sl} = 60^0$.

Figure 10.- Continued.

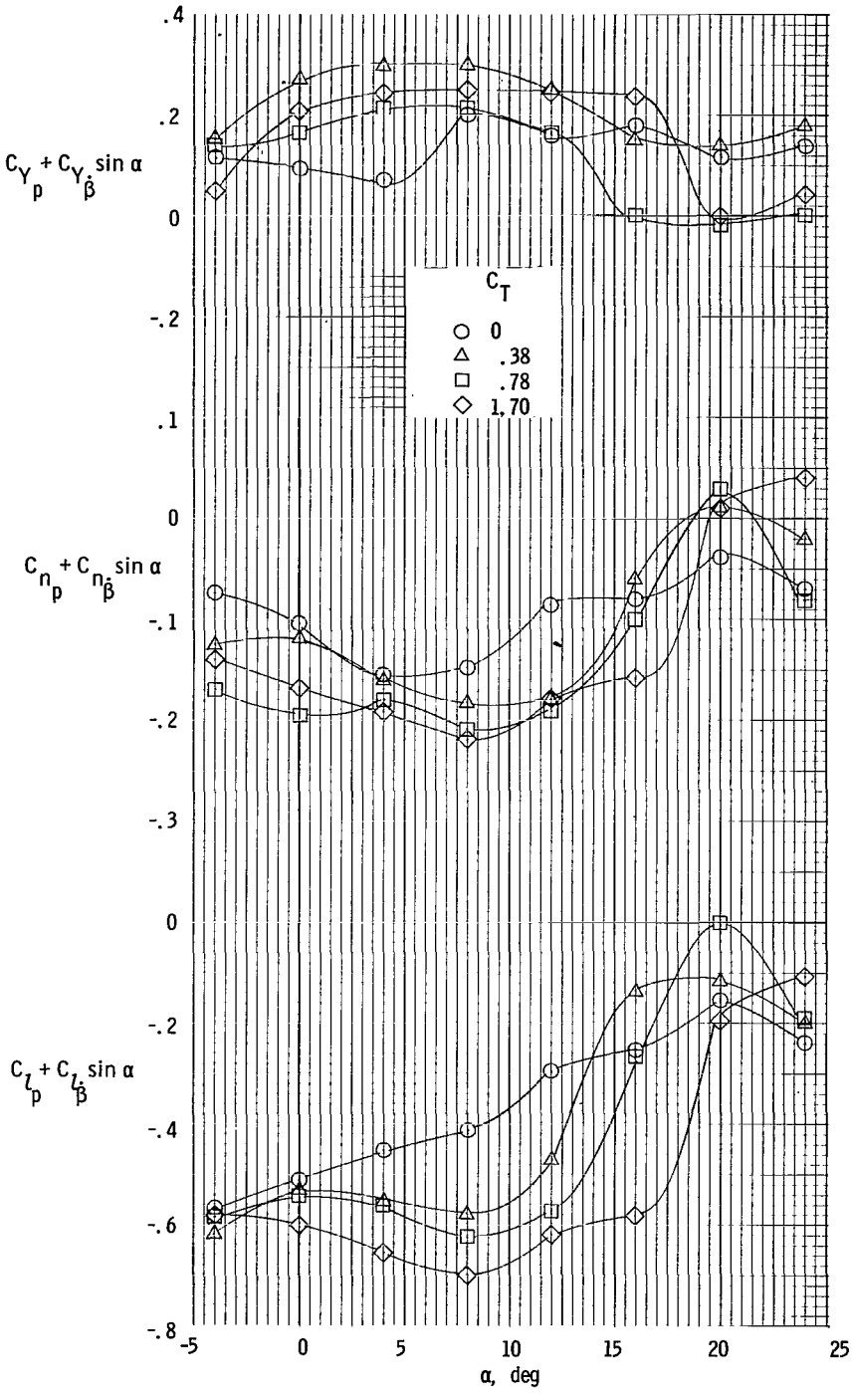

(d) $\delta_{f1}/\delta_{f2} = 30^0/60^0$; $i_t = -9^0$; $\delta_e = 0^0$; $\delta_{sl} = 60^0$.

Figure 10.- Concluded.

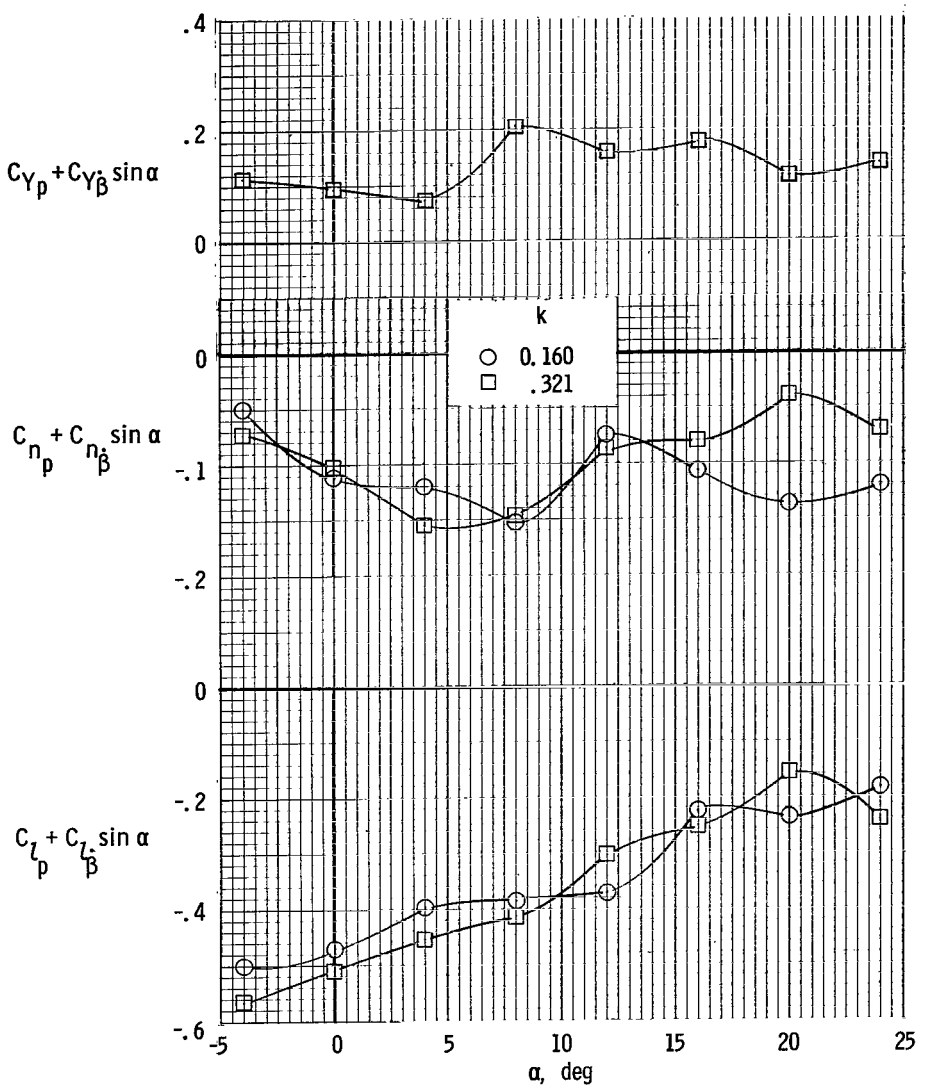

(a) $C_T = 0.$

Figure 11.- Effect of frequency on dynamic rolling derivatives. $\delta_{f1}/\delta_{f2} = 30^0/60^0$; $i_t = -9^0$; $\delta_e = 0^0$; $\delta_{sl} = 60^0$.

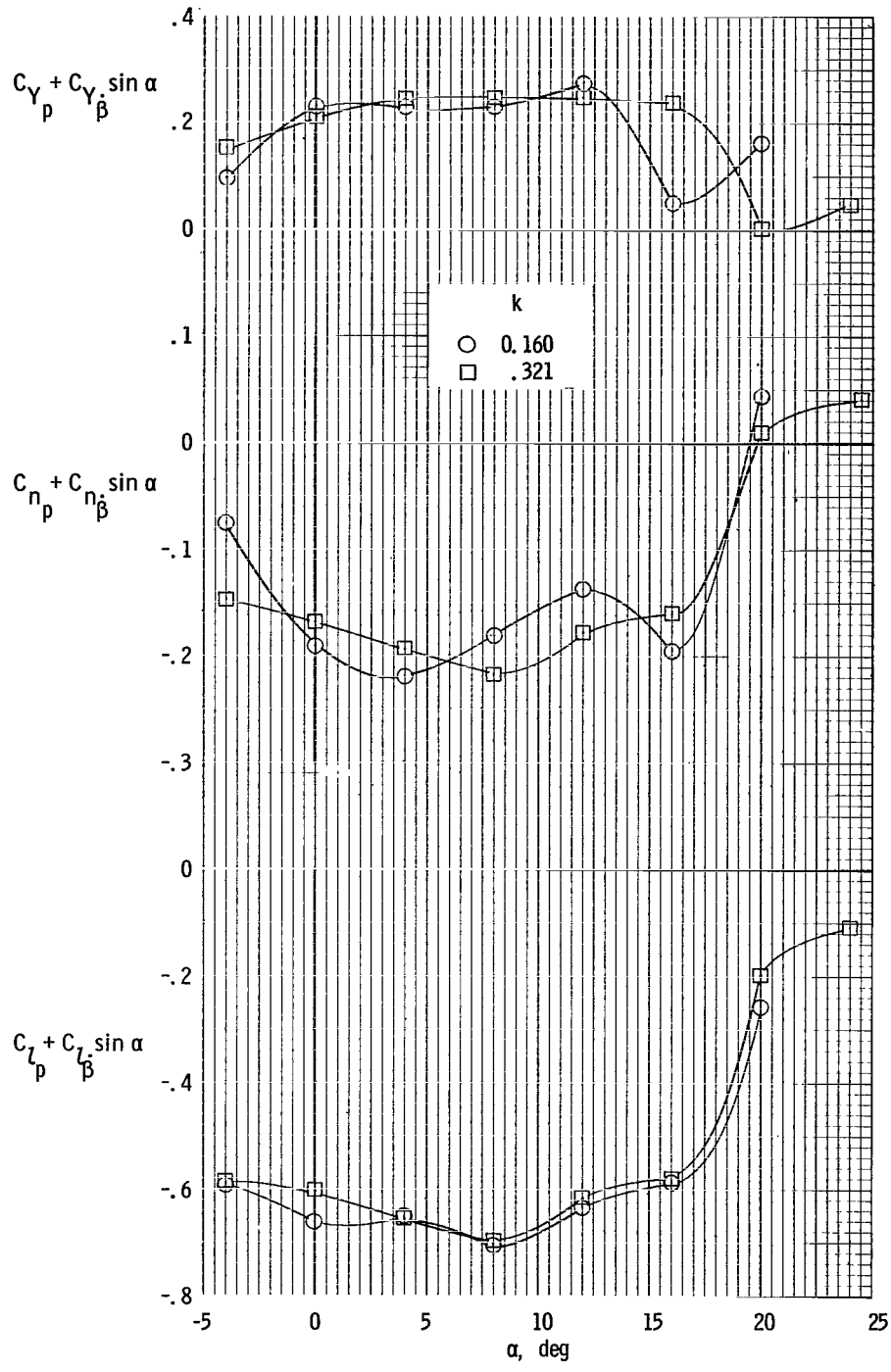

(b) $C_T = 1.70$.

Figure 11.- Concluded.

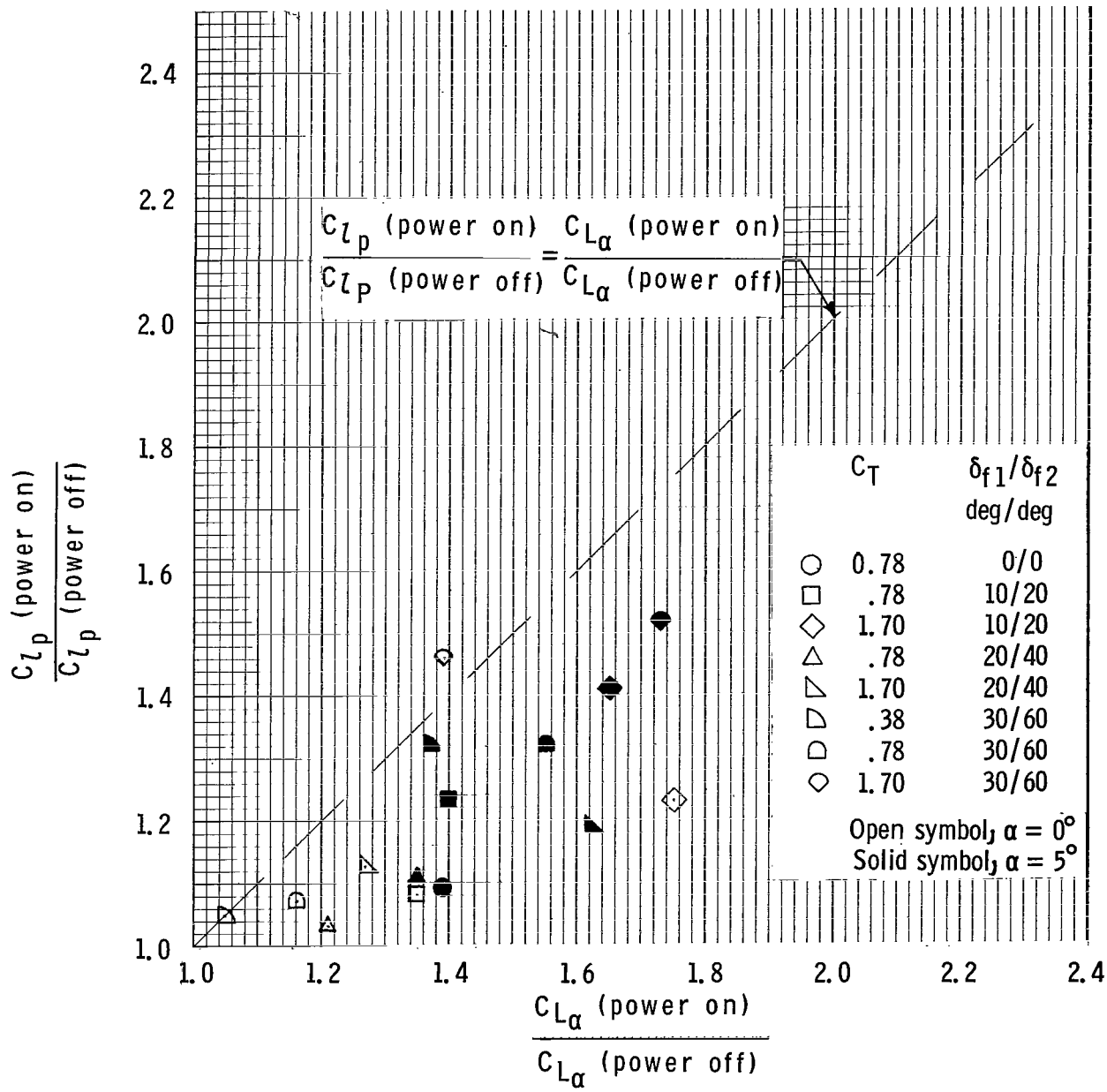

Figure 12.- Increase in roll damping compared with increases in lift-curve slope due to jet-augmented-flap operation.

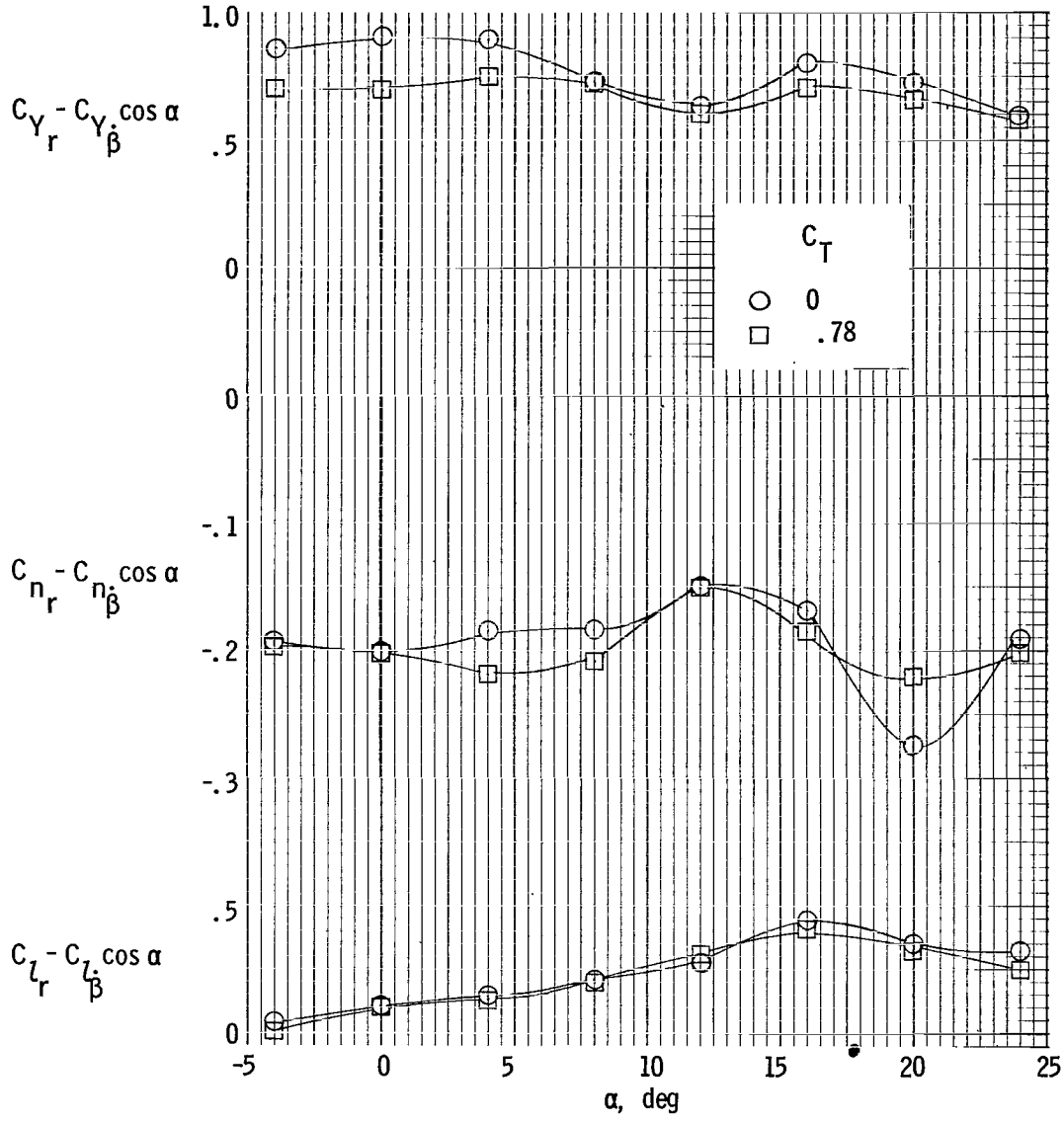

(a) $\delta_{f1}/\delta_{f2} = 0^0/0^0$; $i_t = 0^0$; $\delta_e = 0^0$; $\delta_{sl} = 0^0$.

Figure 13.- Variation of lateral oscillatory yawing derivatives with angle of attack. k = 0.321.

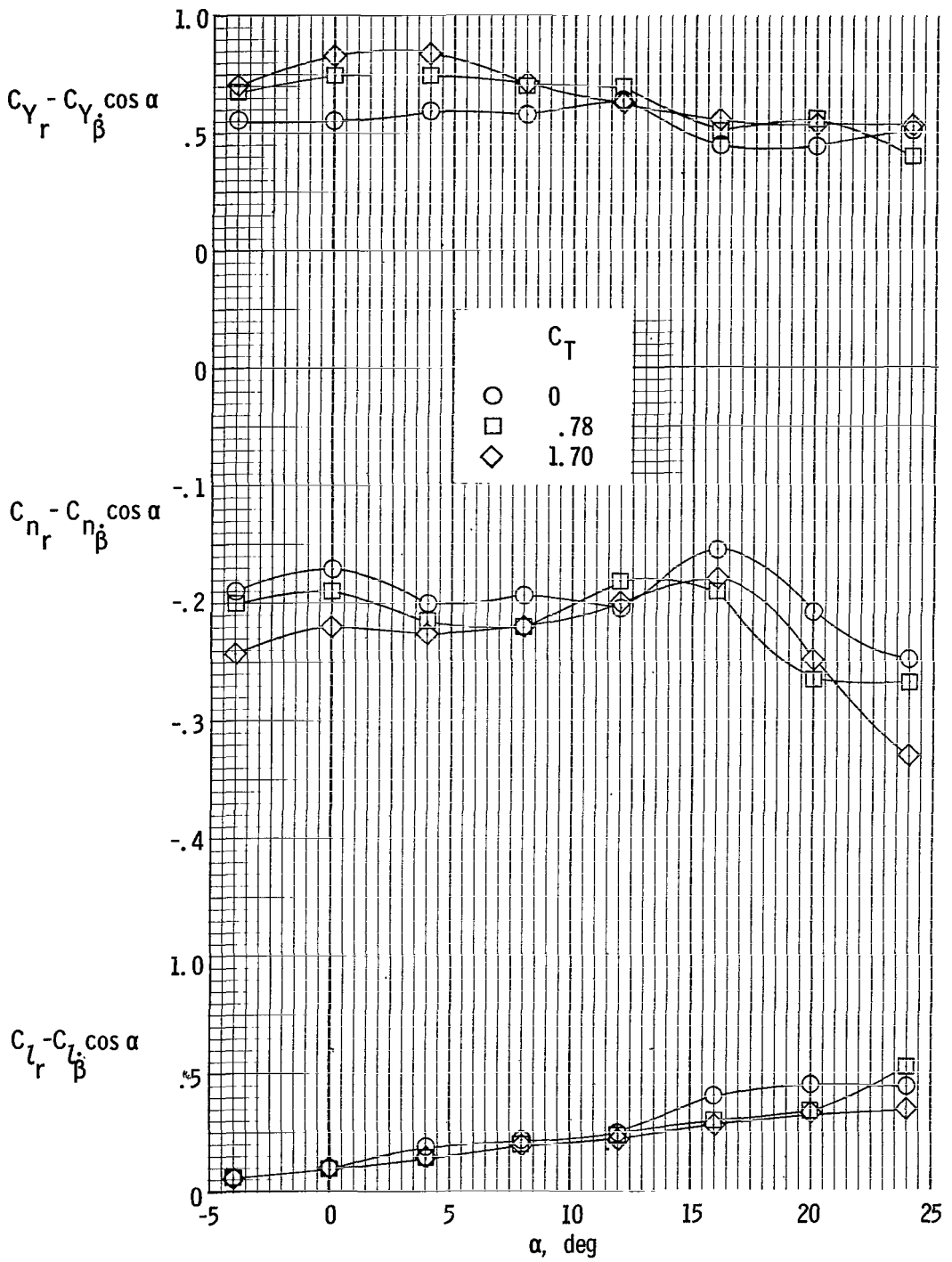

(b) $\delta_{f1}/\delta_{f2} = 10^0/20^0$; $i_t = 0^0$; $\delta_e = -10^0$; $\delta_{sl} = 50^0$.

Figure 13.- Continued.

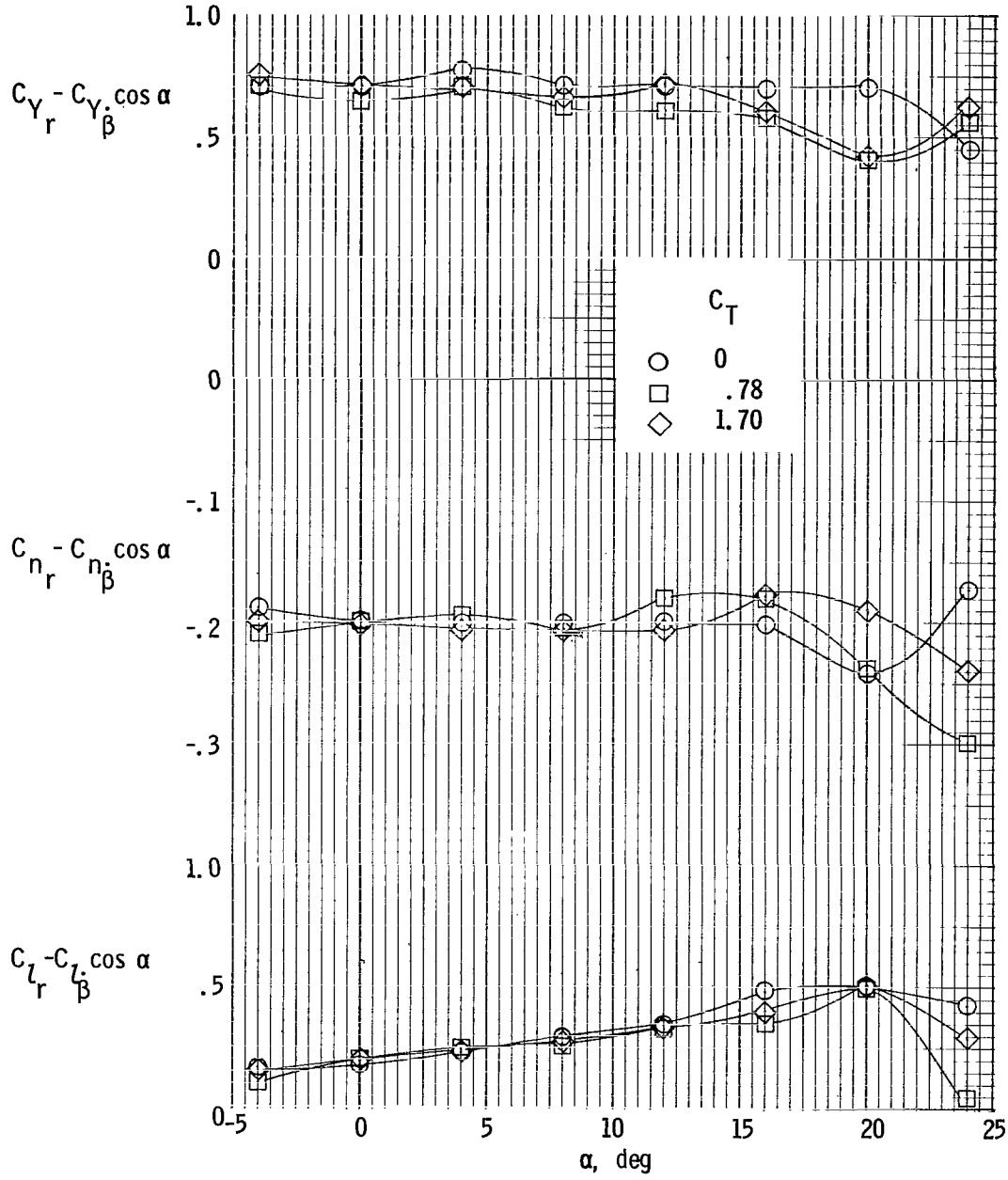

(c) $\delta_{f1}/\delta_{f2} = 20^o/40^o$; $i_t = -5^o$; $\delta_e = -10^o$; $\delta_{sl} = 50^o$.

Figure 13.- Continued.

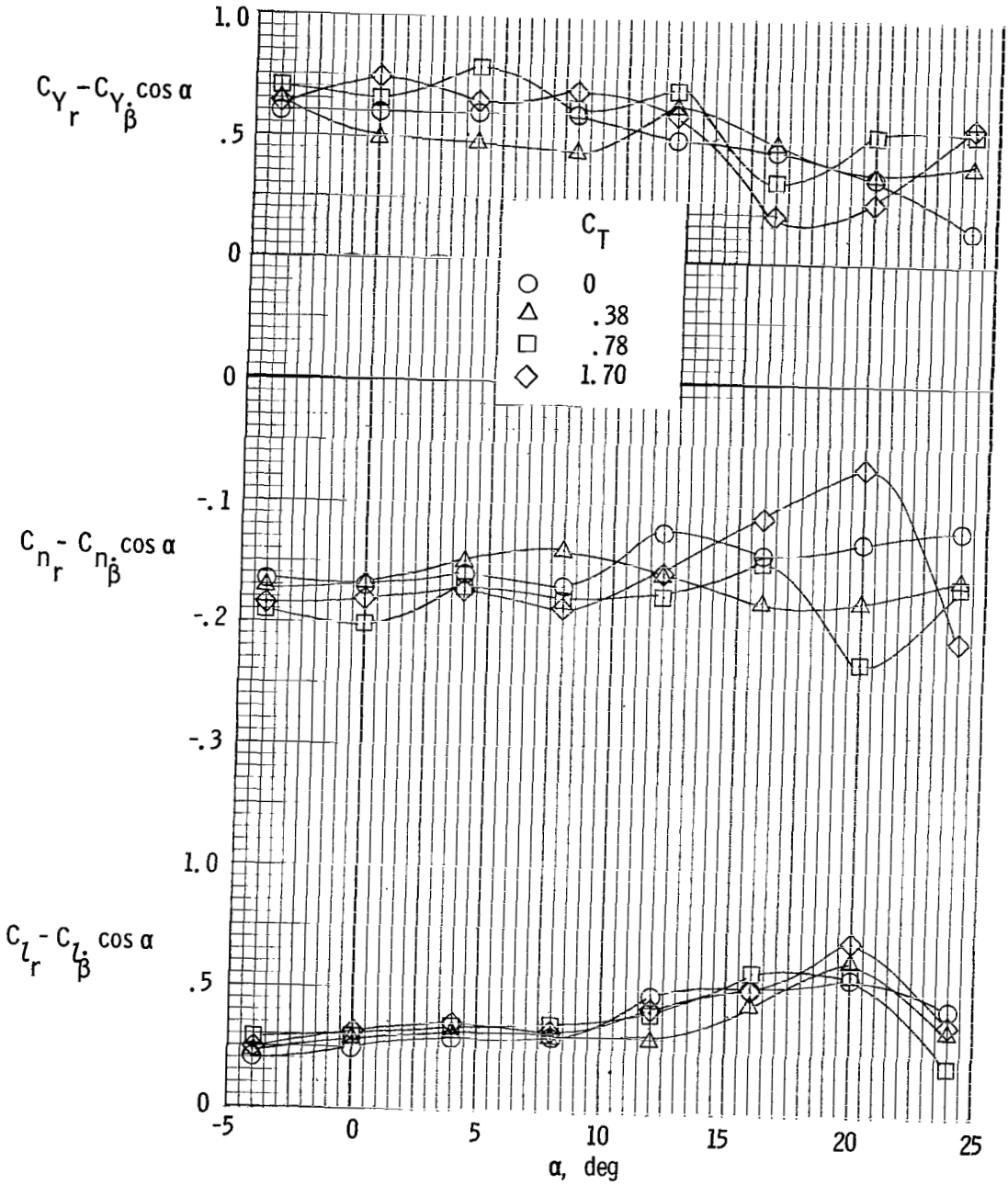

(d) $\delta_{f1}/\delta_{f2} = 30^0/60^0$; $i_t = -9^0$; $\delta_e = 0^0$; $\delta_{sl} = 60^0$.

Figure 13.- Concluded.

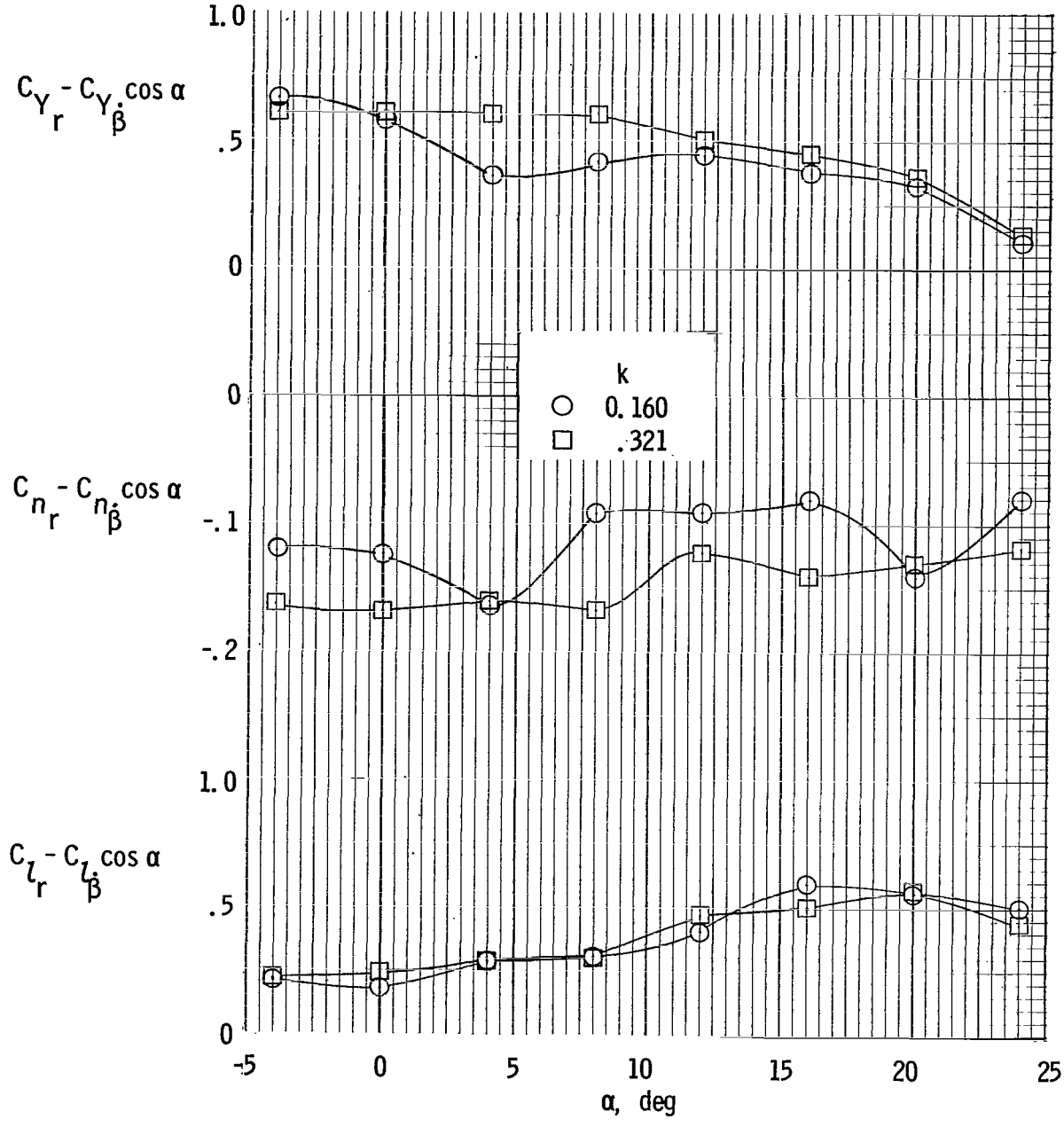

(a) $C_T = 0$.

Figure 14.- Effect of frequency on dynamic yawing derivatives. $\delta_{f1}/\delta_{f2} = 30^0/60^0$; $i_t = -9^0$; $\delta_e = 0^0$; $\delta_{sl} = 60^0$.

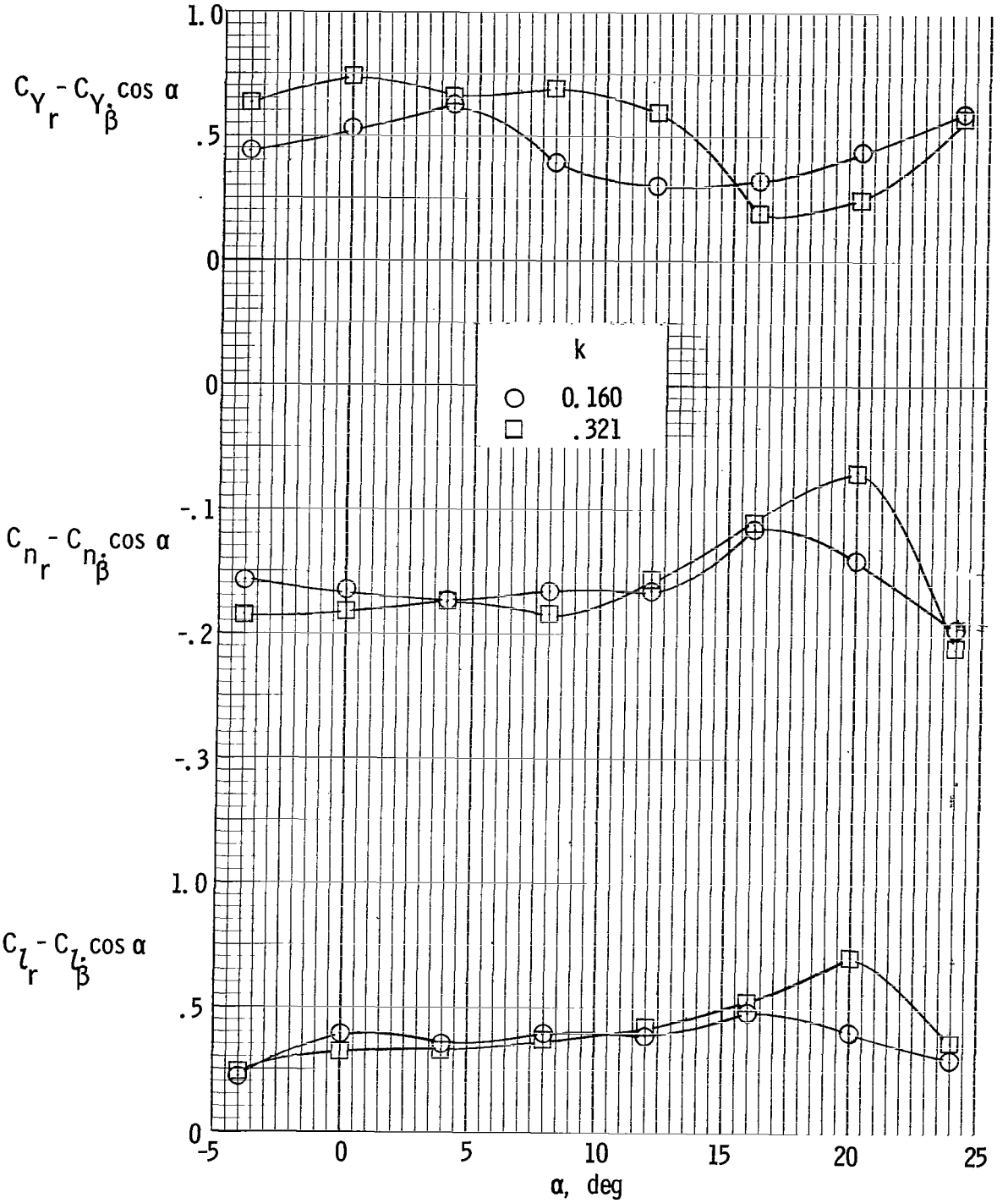

(b) $C_T = 1.70$.

Figure 14.- Concluded.

NASA-Langley, 1969 — 2 L-6521

NATIONAL AERONAUTICS AND SPACE ADMINISTRATION
WASHINGTON, D.C. 20546
OFFICIAL BUSINESS

FIRST CLASS MAIL

POSTAGE AND FEES PAID
NATIONAL AERONAUTICS AN
SPACE ADMINISTRATION

POSTMASTER: If Undeliverable (Section 158 Postal Manual) Do Not Return

"The aeronautical and space activities of the United States shall be conducted so as to contribute . . . to the expansion of human knowledge of phenomena in the atmosphere and space. The Administration shall provide for the widest practicable and appropriate dissemination of information concerning its activities and the results thereof."

—NATIONAL AERONAUTICS AND SPACE ACT OF 1958

NASA SCIENTIFIC AND TECHNICAL PUBLICATIONS

TECHNICAL REPORTS: Scientific and technical information considered important, complete, and a lasting contribution to existing knowledge.

TECHNICAL NOTES: Information less broad in scope but nevertheless of importance as a contribution to existing knowledge.

TECHNICAL MEMORANDUMS: Information receiving limited distribution because of preliminary data, security classification, or other reasons.

CONTRACTOR REPORTS: Scientific and technical information generated under a NASA contract or grant and considered an important contribution to existing knowledge.

TECHNICAL TRANSLATIONS: Information published in a foreign language considered to merit NASA distribution in English.

SPECIAL PUBLICATIONS: Information derived from or of value to NASA activities. Publications include conference proceedings, monographs, data compilations, handbooks, sourcebooks, and special bibliographies.

TECHNOLOGY UTILIZATION PUBLICATIONS: Information on technology used by NASA that may be of particular interest in commercial and other non-aerospace applications. Publications include Tech Briefs, Technology Utilization Reports and Notes, and Technology Surveys.

Details on the availability of these publications may be obtained from:

SCIENTIFIC AND TECHNICAL INFORMATION DIVISION

NATIONAL AERONAUTICS AND SPACE ADMINISTRATION

Washington, D.C. 20546